Journal of Materials Chemistry A

ROYAL SOCIETY OF CHEMISTRY

REVIEW

View Article Online
View Journal | View Issue

Cite this: J. Mater. Chem. A, 2022, 10, 9248

On the mineralization of nanocellulose to produce functional hybrid materials†

Luis Valencia, *[a] Rishab Handa,[b] Susanna Monti,[c] Alma Berenice Jasso-Salcedo,[d] Dimitrios Georgouvelas,[e] Ilse Magaña,[d] Ramón Díaz de León,[d] Krassimir P. Velikov, [fgh] Aji P. Mathew [e] and Sugam Kumar*[i]

Received 17th January 2022
Accepted 31st March 2022

DOI: 10.1039/d2ta00457g

rsc.li/materials-a

Nanocellulose (NC)-based materials constitute a new class of bio-based building blocks that are inspiring advances for the next generation of high-performance sustainable materials. However, NC exhibits important drawbacks which limit its applications, such as its inherent interaction with bacteria and proteins, low conductivity, poor thermal stability, high water absorption (leading to, among other things, loss of structural integrity), *etc.* An efficient strategy to improve this, besides the possibility of introducing further properties, is through mineralization by *in situ* growing inorganic subcomponents to form NC-based hybrids. Following the example of nature which has been mineralizing biopolymers from the beginning of life to create complex structures (forming protective shields or structural supports), mineralization can be adopted in different (2D/3D) configurations, for instance, membranes, scaffolds, sponges, and monoliths (as per requirements), by *in situ* growing multiple subcomponents such as metal oxides, silicates, and metal–organic frameworks. The components act synergistically complementing

[a]*Biofiber Tech Sweden AB, Norrsken House, Birgen Jarksgatan 57 C, Stockholm, SE11356, Sweden. E-mail: luis.valencia@biofibertech.com; luisalex_val@hotmail.com*

[b]*Experimental Physics, Saarland University, Saarbrücken, 66123, Germany*

[c]*CNR-ICCOM–Institute of Chemistry of Organometallic Compounds, via Moruzzi 1, Pisa, 56124, Italy*

[d]*Division of Materials and Environmental Chemistry, Stockholm University, Frescativägen 8, Stockholm, 10691, Sweden*

[e]*Research Center for Applied Chemistry, Blvd Enrique Reyna 140, San José de los Cerritos, Saltillo, Coahuila, 25294, Mexico*

[f]*Soft Condensed Matter & Biophysics, Debye Institute for Nanomaterials Science, Utrecht University, Princetonplein 1, 3584 CC Utrecht, the Netherlands*

[g]*Unilever Innovation Centre Wageningen, Bronland 146708, WH, the Netherlands*

[h]*Institute of Physics, University of Amsterdam, Science Park 904, 1098 XH Amsterdam, the Netherlands*

[i]*Solid-State Physics Division, Bhabha Atomic Research Centre, Mumbai, 400 085, India. E-mail: sugam@barc.gov.in*

† Electronic supplementary information (ESI) available: Table summarizing the main characterization techniques to evaluate nanocellulose-based hybrid materials. See DOI: 10.1039/d2ta00457g

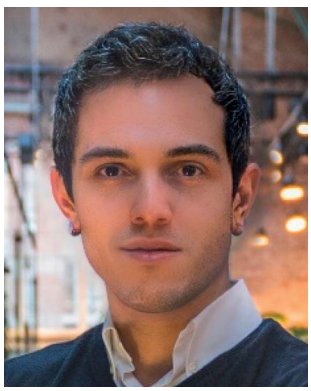

Luis Valencia holds a PhD in Materials Chemistry from Stockholm University (Sweden) and a dual Master's degree in Polymer Science from Strasbourg University (France) and the University of Freiburg (Germany). Luis' research interest lies within the intersection of Polymer Chemistry and Nanotechnology, with the aim of transitioning current materials towards more sustainable paths. Besides his academic studies and multiple research internships in world-renowned institutes, Luis' main activities are within industrial product development, and he currently holds the role of Director - Material Development & Application Lead in Biofiber Tech Sweden.

Sugam Kumar received his M.Sc. in Physics from Aligarh Muslim University in 2007 and joined Bhabha Atomic Research Centre, Mumbai, India as a Scientific Officer in 2009. He obtained his PhD from Homi Bhabha National Institute, Mumbai, India in 2015 and carried out his postdoctoral research between 2017 and 2019 at Stockholm University, Sweden. His research interests deal with the understanding of an interplay of interactions in multicomponent soft matter systems, including biomolecules, polymers, amphiphiles, and nanomaterials for exploring the pathways to design hybrid materials.

each other, thus providing new functionalities that the components individually do not possess. For instance, it is possible to introduce properties such as self-healing behavior, magnetic character, antimicrobial properties, electrical and thermal conductivity, *etc.*, which opens a wide range of opportunities in a variety of fields (*e.g.*, energy, printed electronics, biomedicine, water/gas purification, *etc.*) of current interest and requirements. The present review paper summarizes and discusses the advanced applications of thus-formed nanocellulose hybrids, along with a general overview of the synthesis protocol and advanced characterization tools used to analyze these complex materials.

1. Introduction

From the birth of the universe, nature during evolutionary processes has produced *via* biomineralization a multitude of fascinating hybrid materials that, with remarkable elegance and efficiency of structures, combine organic and inorganic components at the nanoscale, synergistically combining their properties at the macroscale. Over the last few decades, scientists have followed the example of nature and developed synthetic hybrid materials by merging the properties of biopolymers, optimized by evolution, with those of synthetic components, leading to the elaboration of materials with unique characteristics and applications.

A type of biopolymer that has attracted the attention of materials scientists over the last few decades is nanocellulose (NC). NC-based materials exhibit an unprecedented combination of properties, which leads to, among many other advantages, excellent mechanical properties, the capability to support cell growth, and versatile surface chemistry to tailor functionalities.[1–4] Therefore, NC-based materials constitute a new class of bio-based "building blocks" that are inspiring advances for the next generation of high-performance sustainable materials. NC materials can help satisfy the current demand for products made from renewable and sustainable resources with low environmental impact and low safety risks to animal/human health.[5]

The macromolecular architectures provided by NC constitute precious backbones or templates for the fabrication of hybrid materials. Mineralization of structures with subcomponents such as metal oxides, silicates, and metal–organic frameworks is possible through the chemical modification of the abundant hydroxyl groups present on the surface of NC, making it an attractive path towards the optimal expression of properties brought together by multiple components in one single material. The hybrids thus formed by mineralization of NC can possess several unique and promising characteristics like self-healing, magnetic character, and antimicrobial properties, as well as electrical and thermal conductivity, which can be exploited to develop smart materials, opening a wide range of opportunities in a variety of fields (*e.g.*, energy,[6] printed electronics,[7,8] biomedicine,[9,10] water/gas purification,[11,12] catalysis,[13–15] *etc.*). The mineralization can be adopted in different configurations, for instance, membranes, scaffolds, sponges, and monoliths, as per requirements. The unique characteristics and their implementation for emerging applications have therefore stimulated intense scientific research efforts in the hybridization of nanocellulose.

The current review paper summarizes and discusses the recent interesting applications of nanocellulose hybrids, focusing on the literature from the last five years. It is however impossible to completely describe this field in a single review; therefore, this article provides the reader a general overview of the main applications of the hybrid materials formed *via* mineralization along with a discussion of the synthesis procedure, properties, and advanced characterization tools used to analyze these complex materials. Selected representative examples are described in detail.

2. Nanocellulose (NC)

Cellulose, which is considered the most abundant organic raw material on Earth, is composed of hundreds to millions of glucose units connected with β-1,4-glycosidic bonds that give rise to a high molecular weight homopolysaccharide.[16] In nature, cellulose is found as yarns composed of numerous individual fibers assembled in hierarchical order. Intramolecular and intermolecular forces generate larger units known as elemental fibrils (protofibrils), which are packed into units called microfibrils. The hydroxyl (–OH) groups of the glucose units represent active sites for modifications due to their high reactivity. Cellulose-based materials stand out due to their low cost, low density, low carbon footprint, and biodegradable and renewable nature.[17]

Cellulose particles can be extracted from a wide range of sources, varying in size, chemical composition, and other properties such as crystallinity. In the last few decades, NC, *i.e.*, cellulose in the form of nanostructures, has been proven to be one of the most prominent green materials and has attracted extensive research and industrial interest.[18,19] Two main types of nanocellulose can be extracted from cellulose, as schematically shown in Fig. 1, differing in the steps involved in their isolation and their structure.[1,19–22]

Cellulose nanofibrils (CNFs) are flexible ribbons obtained by mechanical treatment of cellulose fibers, composed of alternating amorphous and crystalline domains. They can be produced from different sources *via* mechanical disintegration with high-shear processes such as grinding, microfluidization, and homogenization. CNFs possess a high aspect ratio ($\approx$100) with dimensions of 2–60 nm in diameter and a few microns in length, depending on the processing method.[23–25]

Cellulose nanocrystals (CNCs) are rigid rod-like particles obtained by chemical treatment of cellulose, mainly acid hydrolysis of the amorphous parts using sulfuric acid. CNCs are primarily crystalline, with a length of 100–1000 nm and a diameter of 2–20 nm. The dimensions vary depending on the

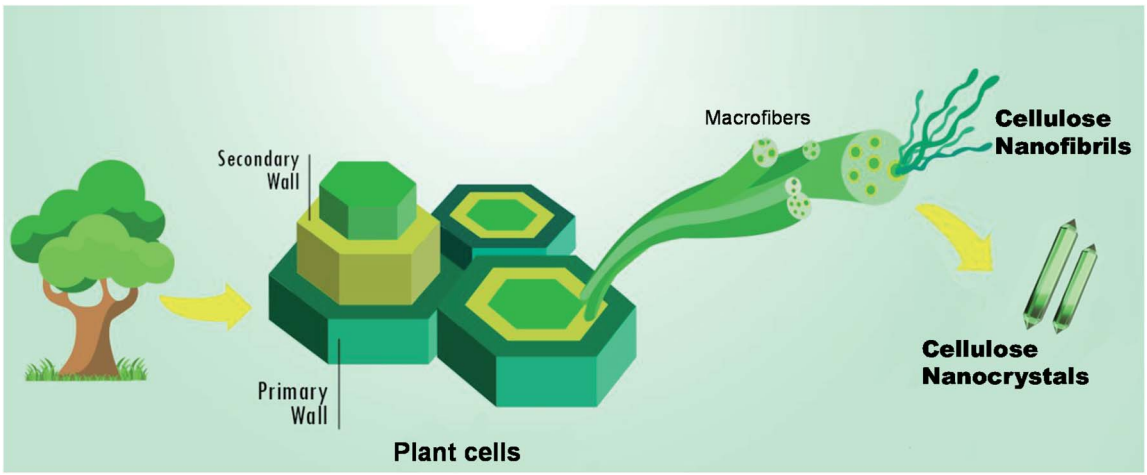

Fig. 1 Conceptual schematic representation of the hierarchical structure of cellulose from trees.

source from which they are obtained, as well as the preparation conditions. Another characteristic of CNCs is that they can organize in a chiral nematic manner in suspensions leading to the formation of iridescent films when dried, unlike CNFs.[1,26–28]

It is worth mentioning that, besides CNFs and CNCs, bacterial cellulose (BC) is also a very important cellulose-based nanomaterial that allows the creation of products with a good level of performance. BC is synthesized by bacteria and exhibits diameters of around 20–100 nm. Although this article is mainly focused on CNFs and CNCs, we do provide some selected examples of BC-based hybrid materials, and we recommend the reader the review by Gorgieva *et al.* for further details about this topic.[29]

3. Nanocellulose mineralization

3.1. Mineralized materials in nature

Nature has employed mineralization for producing a variety of materials that have the ability to perform amazing functions and possess unique properties. These materials are usually formed at ambient physiological conditions by arranging soft and hard phases in complex hierarchical architectures, with a fairly limited number of sub-components. The materials are often lightweight with characteristic dimensions ranging in the nano- to macroscale and exhibit different levels of strength and flexibility.[30] There are several examples of natural mineralized materials such as mollusk shells, the skeleton of sea urchins, bone, teeth, algae, biogenic silica, *etc.*,[31] some of which are described in brief below.

• **Bone.** The bone comprises mineralized collagen fibrils as a basic building block, where the plate-shaped nanocrystals of carbonated hydroxyapatite are embedded in a collagen framework. The mechanical properties of the bone are largely determined by the number of minerals in the tissue.

• **Teeth.** The mammalian tooth consists of a hard component, enamel, which is supported by the less mineralized and more resilient connective tissue dentin, formed from and supported by the dental pulp. Enamel is highly mineralized tissue, composed of around 97% mineral (w/w), ~1% organic material, and ~2% water.

• **Calcified cartilage.** Calcified cartilage is a highly mineralized thin interlayer between the hyaline articular cartilage and the subchondral bone, participating in transmitting mechanical stress and biological stimuli from the hyaline cartilage to the bone. This is largely constituted of collagen as an organic compound and hydroxyapatite as an inorganic component.

• **Mollusk shells.** Shells are largely made up of calcium carbonate forming multi-layered microstructures, along with a small amount of organic component. Due to the microstructure of the composite, these shells show an increase in toughness by around three orders of magnitude compared to that of non-biogenic calcium carbonate.

• **Nacre.** The nacreous layer is composed of aragonite polygonal tablets, arranged in a laminated structure between thin sheets of the organic matrix, of some biopolymers such as silk proteins and polysaccharides. The mixing of the brittle tablets and the thin layers of biopolymers in laminate configuration provide mechanical strength and enhanced toughness, and make the material resilient.

• **Algae and diatoms.** The cell wall of most algae is largely made up of organic components such as cellulose, hemicellulose, mucilage, pectin, *etc.* mineralized with calcium carbonate, silica, *etc.*, in different combinations for different algae. Diatoms which represent a large group of several genera of algae contain a cell wall made up of silica (siliceous shells).

• **Magnetotactic bacteria.** These refer to a polyphyletic group of bacteria having the ability to orient themselves along the magnetic field lines of Earth. These bacteria possess organelles called magnetosomes that contain magnetic crystals such as Fe_3O_4 and Fe_3S_4.

Scientists are interested in exploring these naturally mineralized materials to follow the designs and protocols of nature for assembling or disassembling the building block efficiently to generate materials that can mimic natural structures.[30,32,33] There are certainly interesting as well as usually common observations about the structures and building blocks of these

materials.[34–36] For example, (i) these materials usually display the formation of organized hierarchical structures at a range of scales from molecular to macroscopic levels. By studying the self-similar structure of the composite, mimicking the bone structure, it has been shown that the hierarchical organization contributes to the robustness of these materials.[34] (ii) The building blocks of these materials are generally nanomaterials, assembled through nanofabrication methodologies. It has been shown that the composite in nature shows a generic mechanical structure, where the nanometer size of the particles ensures optimum strength and maximum tolerance to flaws (robustness).[34] (iii) Most of the time the building block possesses anisotropic geometry and is dispersed in a matrix of soft molecules. For instance, enamel consists of rod-like nanocrystals, with low soft protein content. The anisotropy of the building blocks can explain the stiffness of the natural mineralized materials such as bone in spite of the low mineral content.[34] It should however be mentioned that the overall response of the material is required to be isotropic, despite the anisotropic character at some hierarchical level.

Considering all the above points, it is worth concluding that nanocellulose can serve as a building block for fabricating artificial mineralized materials, due to its properties, such as nanometer size, anisotropy in structure, ability to form a self-organized hierarchical structure and ability to play the role of the soft matrix.

3.2. Scope and motivation of NC mineralization

Even though nanocellulose exhibits amazing properties and capabilities, several challenges limit its implementation in multiple applications, such as its inherent interaction with bacteria and proteins (leading to surface fouling), poor thermal stability, loss of structural integrity due to water-induced swelling, low conductivity, high flammability, and poor compatibility with polymer matrixes.[17,37] Moreover, despite its anionic groups, *e.g.*, carbonyl or sulphate/phosphate (depending on the acid used in the hydrolysis process (for CNC extraction)), on the surface, pristine NC does not offer enough functionality for water/gas separation, so the NC-based membranes/filters are not sufficiently good to solve the current water pollution problems. Nevertheless, NC has very good processability into different porous materials, which can serve as templates to *in situ* grow functional nanoparticles that impart further properties to the resultant hybrid material. Upon the mineralization processes, the components act synergistically complementing each other, thus providing new functionalities that the components individually do not possess.

The physical properties of the mineralized materials will essentially depend on the chemical composition of the phases (nanocellulose + metal–organic frameworks/metal oxide nanoparticles, *etc.*), and the processing method/conditions to form the final 2D/3D material. Any further interaction among the components that form the hybrid (chemical or physical cross-linking) can be furthermore used to tune the properties of the final material. Different hybridization strategies can be carried out depending on the desired end-use, for instance, to provide mechanical reinforcement,[38] to enhance/prevent cell-adhesion and cell-proliferation,[39] or to tailor specific functionalities.

Another important aspect in the tailoring of hybrid networks concerns the chemical pathways that are used to design a given hybrid material. Most mineralization processes are carried out *via* depositing the inorganic materials through vapor (*e.g.*, chemical vapor deposition, atomic layer deposition, magnetron sputtering, or inkjet-printed coating) or in solution (sol–gel chemistry).[16] A very convenient route is *via* conventional sol–gel chemistry, for instance (i) *via* hydrolysis of organically modified metal alkoxides or metal halides; (ii) using specific bridged precursors such as silsesquioxanes and polyfunctional precursors, or (iii) *via* hydrothermal synthesis in polar solvents.[40–43] The deposition through vapor is efficient but leads to a large number of inhomogeneities. Deposition through solution, on the other hand, leads to better homogeneity; however, the tight network of nanocellulose can make it impenetrable for solvent molecules, especially when organic solvents are required. A possible solution for this is to mineralize through "inclusion", in which cellulose can be dissolved in ionic liquids before mineralization.[44] Furthermore, besides a vast amount of hydroxyl groups, nanocellulose has anionic groups such as sulfate and carboxylate, which enhance the adsorption capacity of metals.[45] The mineralization of MOFs is based on this cellulose–metal interaction, as it can proceed by the addition of linkers that act as MOF precursors and are exposed to standard solvothermal and hydrothermal methods. The authors recommend the recent review by Abdelhamid *et al.*, which explains this topic in detail.[40]

It's important to differentiate mineralization (*in situ* hybridization) processes from other types of *ex situ* hybridization routes. *Ex situ* hybridization refers to those processes in which the components of the hybrid material are synthesized/extracted separately and mixed to undergo chemical/physical bonding between them in the nanoscale (as opposed to composites where the components are mixed at the macro level, *e.g.*, matrix + reinforcing additive or filler). On the other hand, *in situ* hybridization (mineralization) refers to the growth of one or multiple subcomponents from the surface of the substrate (in this case, nanocellulose), thus having strong chemical bonding between the different phases.

Mineralization processes are especially advantageous/attractive functionalization routes for biopolymers such as nanocellulose because of the following reasons: (i) NC offers a high and highly reactive surface area favoring the formation of porous structures. The combination of both properties allows high loadings of mineralized nanoparticles and therefore a high level of functionality. (ii) Mineralization processes can also be used to imprint the unique signatures of cellulose nanocrystals (helically ordered rod-like structure and entropic topological constraints) onto inorganic nanoparticles when mineralizing a CNC suspension in the chiral nematic phase.[46,47] The nanocellulose phase can be removed for instance *via* calcination to obtain templated inorganic nanoparticles.[48] However, this is beyond the scope of this article, where we focus on materials, retaining nanocellulose as the main component. (iii) As stated earlier, mineralization can be used to induce several unique

properties in nanocellulose, which are otherwise not present, such as thermal stability, flame resistance, antimicrobial activity, photocatalytic activity, electrical conductivity, wear and abrasion resistance, magnetic character, *etc.*, useful for a range of applications (discussed in later sections of the article). (iv) *In situ* mineralization can also be useful in imparting secondary properties to the nanocellulose matrix. For example, purification of aqueous solutions from metal ions using NC membrane can give rise to the formation of metal/metal oxide nanoparticles in the NC matrix, resulting in added advantages of antimicrobial and photocatalytic activities.[49] (v) Mineralization of NC can be carried out at ambient or near ambient conditions utilizing simpler, cost-effective, and scalable green chemistry methods. (vi) Moreover, the bioinspired mineralization of nanocellulose can be employed for developing materials having properties analogous to those of their natural counterparts. For instance, inspired by the structure of bone, *in situ* mineralization of bacterial cellulose, aligned by the stretching process, was carried out to produce materials having high elastic modulus and hardness comparable to mouse trabecular bone.[50,51] Similarly, by drawing inspiration from several properties (*e.g.*, organic–inorganic composite, 3D porous structures, cytocompatibility, *etc.*) of naturally mineralized materials, Wu *et al.* fabricated a scaffold *via in situ* biomimetic mineralization of the hydroxyethyl cellulose/soy protein isolate and hydroxyapatite for bone defect repair. The synthesized scaffolds possess interconnected porous structures, with improved mechanical properties and controllable degradation rate, as well as a calcium/phosphorus ratio (1.65) almost equivalent to that of natural bone tissue (1.67).[52] Mohammadi *et al.* reported the design strategy for a mineralized biocomposite that can have complex shapes of dental implant crowns, drawing inspiration from the impact-resistant dactyl club of the stomatopod. This material consists of a self-assembled chiral nematic structure of CNCs, mixed with genetically engineered proteins, that can bind with CNCs as well as regulate the *in situ* growth of apatite crystals. The synthesized bioinspired composite manifests high strength, stiffness, and fracture toughness, along with a graded microstructure, resembling that seen in naturally mineralized materials, *e.g.* human teeth or the stomatopod dactyl club.[53] In another study, mineralized oral films able to provide ions required for remineralization of early demineralized tooth lesions were prepared using hydroxyethyl cellulose, cellulose nanofibers, and nepheline fluorapatite glass powder.[54] A nature-inspired strategy has been reported to fabricate superhydrophobic cotton fabric possessing unique features such as resistance to ultraviolet irradiation as well as to mechanical wear and abrasion, high temperature, organic solvent immersion, *etc.*[55] An electrochemical sensing device having the capability of *in situ* sensing of chiral molecules has been developed by mineralization of wood membrane by Prussian blue, taking inspiration from nature's protocol of mineralizing wood.[56]

Besides the conventional mineralized inorganic materials on biopolymers, multiple other subcomponents have been recently explored for mineralizing NC, targeting different applications. The main candidates are metal/metal oxide nanoparticles, metal–organic frameworks, and bioactive glass, as further described below. A representative SEM micrograph of these different nanomaterials is shown in Fig. 2.

Metal nanoparticles (MNPs) such as gold (Au), silver (Ag), nickel (Ni), ruthenium (Ru), palladium (Pd), platinum (Pt), copper (Cu), and iron (Fe) nanoparticles (NPs) are important in many fields owing to their unique optical, electrical, and antibacterial properties besides good catalytic effects.[57] MNPs can be prepared by electrochemical methods, thermal decomposition, electromagnetic irradiation, sol–gel chemistry, and chemical reduction methods. MNPs usually become thermodynamically unstable and tend to aggregate due to their large specific surface area. NC has been reported to promote the nucleation of nanoparticles due to its good stabilizing effect for MNPs, besides preventing their agglomeration.[58] The development of NC/MNP hybrid materials is an excellent way to obtain high-performance materials, loading or assembling various MNPs on NC *via* chemical reduction,[59] reduction by UV irradiation, and thermal reduction synthesis.[60] The applications of these hybrid materials include plasmonic sensors,[61] wound dressings,[62] visual detection of volatile compounds,[63] surface-enhanced Raman scattering (SERS) detection,[64] and catalysis.[65]

Metal oxide nanoparticles (MONPs) are considered heterogeneous catalysts having excellent optical properties, as well as antibacterial and magnetic properties (properties varying depending on the type of metal and oxidation state). Examples are zinc oxide (ZnO), magnesium oxide (MgO), titanium dioxide (TiO_2), copper oxide (CuO), *etc.* MONPs have been studied for

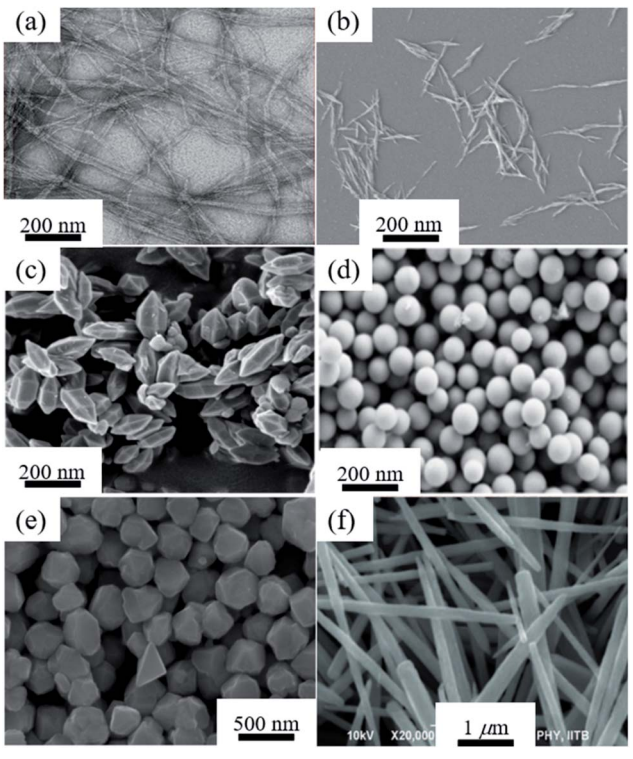

Fig. 2 TEM micrograph of (a) CNFs from bamboo fibers,[93] and SEM micrographs of (b) CNCs isolated from cotton linters,[94] (c) bimetallic FeMn-MOF particles,[95] (d) nanosized bioactive glass particles (nBGPs),[96] (e) copper nanoparticles,[97] and (f) ZnO nanowires.[98]

applications such as biocides, catalysts, electronics, biosensors, optical devices, and healthcare products.[10] Therefore, combining nanocellulose with MONPs makes it possible to synthesize hybrid materials that can be used in drug delivery, bio-separation, packaging, wound healing, or water purification.[10,57,66,67]

Metal–organic frameworks (MOFs), also known as porous coordination polymers (PCPs), have emerged as a new class of porous organic/inorganic hybrid materials, which are constructed by organic linkers and metal nodes.[68,69] These materials constitute a unique large family of crystalline 3D solids that have exceptional characteristics such as extremely high surface area (1000–10 000 $m^2\ g^{-1}$), high porosity, flexible functionality, redox properties, and tunable pore size,[70,71] which give them great versatility for their application in different fields of research which include gas storage,[72] separation,[73,74] catalysis,[75,76] photocatalysis,[77] energy conversion,[78] drug delivery,[79] and opto-electronics,[80] among others. MOFs can be synthesized by different techniques, for instance *via* conventional electric heating, microwave heating, electrochemistry, mechanochemistry, ultrasound-assisted synthesis, sonochemistry, or step-by-step methods.[81,82]

Bioactive glass (BG) is based on the SiO_2–P_2O_5–CaO–Na_2O system and it is considered a very promising material in the biomedical area due to its ability to bond with bone and soft tissues.[83] Moreover, BG also offers bioactivity or a stimulatory effect on osteoblast cell activity (osteogenesis and vascularization) through a combination of surface reactivity and ion release (including soluble silica species, phosphate, and calcium),[84,85] which occurs during the degradation process. A strong bone-to-material bond can be generated by BG due to the formation of a hydroxy-carbonated apatite (HCA) layer on its surface,[86] therefore, it is a material that is quite applicable in bone regeneration/repair,[87] soft tissue regeneration, wound healing, and drug delivery.[84] BG can be mainly produced *via* melt-quenching,[88] microemulsion, flame synthesis, and sol–gel methods,[89,90] with the last giving the possibility of controlling the size and morphology.[87] On the other hand, NC has been studied for tissue engineering due to its biocompatibility and a refined 3D network, which is similar to the shape of collagen nanofibers. By this, investigations have been carried out to develop 3D-BG scaffolds using NC as a template *via* the sol–gel route for biomedical applications.[91,92]

4. Processing strategies of nanocellulose-based materials

The final properties of the hybrid material also depend strongly on the processing pathways, and in this review article we focus on 2D/3-dimensional materials in which NC is the main component. There are big differences between CNFs and CNCs when considered as materials components. For CNFs, a strong network is formed arising from physical interactions between the nanofibers and their long aspect ratio, which makes them an ideal candidate for the fabrication of 2-dimensional (*e.g.*, films/membranes) or 3-dimensional materials (*e.g.*, foams/aerogels, scaffolds, or monoliths). CNCs, on the other hand, do not form as strong materials as CNFs (unless they are surface-modified or crosslinked), due to their stiff rod-like nature. However, they can form iridescent films due to their intrinsic nature of self-assembling into chiral nematic liquid crystals. The strength of the network and thus the resultant materials based on either CNFs or CNCs can be tuned by surface modification (*e.g.*, *via* (2,2,6,6-tetramethylpiperidin-1-yl)oxyl (TEMPO) mediated oxidation (TO)) or *via* physical (*e.g.*, by incorporation of multivalent metal ions) or chemical crosslinking.

Mineralized hybrid materials are processed following conventional processing techniques for nanocellulose, where the material can be either produced using "pre-mineralized" nanofibers or nanocrystals or having produced the material first to then mineralize it with the subcomponent of choice, depending on the application. It's worth mentioning that the mineralization processes can disrupt the hydrogen bonding interactions among the nanofibers/nanocrystals, therefore potentially compromising the mechanical properties of the materials, which can be solved in different ways, for instance introducing another component to form an interpenetrated network.[99]

4.1. 2-Dimensional materials

The fabrication of 2-dimensional materials, here referring to films and membranes, is the most well-established method to process (nano)cellulosic materials, following the example of the paper industry. Due to the higher aspect ratio and strong hydrogen bonding, nanocellulose-based films are much stronger than common paper used for writing, printing, or packaging. Moreover, transparency can also be achieved due to the nanometric size of the particles. Various alignment techniques (such as wet stretching, wet extrusion, and cold drawing) have been developed to enhance the mechanical performance of the films even more. The authors recommend the review by Fang *et al.* for further information on this topic.[100]

Membranes are films with controlled porosity, which can be utilized for separation processes, while the pore size/density can be easily tuned by varying the size (length and diameter) of the fibrils. A typical process to produce nanocellulosic films is *via* vacuum filtration of a nanocellulose suspension, forming a densely packed layer resulting in a wet nanocellulose pad that is subsequently peeled off from the filter and dried under pressure.[101] Another method to obtain nanocellulose films/membranes is by using the casting/evaporation process that consists of the controlled removal of solvent from a suspension containing nanocellulose. Hybrid nanocellulosic films/membranes (also called cellulose nanopapers (CNPs)) obtained by these processes have been investigated for many applications such as water treatment, electronics and photonic devices, and detection of biomolecules upon mineralization.[102–105]

4.2. 3-Dimensional materials

3-Dimensional materials refer to structures built with a significant length in the *z*-axis, besides the *x* and *y* axes. There are

several challenges in the preparation of 3D materials compared to 2D ones, for instance, the challenge of making the *z*-axis show comparable performance to the *x* and *y* axes, considering that the *z*-axis strength depends a lot on the properties of the layer, as well as on the orientation of the subcomponents. Multiple processing techniques have been explored over the last few years to prepare 3-dimensional nanocellulosic materials, such as 3D printing, to form monoliths or scaffolds, freeze-casting, and other foaming methods to prepare foams/aerogels. The inherent porosity of the materials, due to the space gap between the nanofibrils/nanocrystals, enables these 3D materials to be used in gas capture, water purification, and various biomedical applications, among others.

Foams and aerogels are essentially 3D porous materials with ultralow density. These materials exhibit promising potential in a wide range of applications, such as thermal insulation, biomedical scaffolds, and devices for energy storage. The difference between a foam and an aerogel, according to Lavoine *et al.*,[106] lies essentially in the degree of porosity. A foam exhibits a porosity larger than 50% in which gas is dispersed in a liquid, solid, or hydrogel, with pore sizes larger than 50 nm. Aerogels, on the other hand, exhibit porosity higher than 90% and pore sizes ranging between 2 and 50 nm. The processing of nanocellulose-based aerogels/foams, though there are several reported methods, basically relies upon careful solvent removal from an NC suspension. This can be done *via* different methods (*e.g.*, oven drying, freeze-drying, and supercritical drying preceded by solvent exchange), while the resultant foam properties will dramatically depend on the processing conditions, varying the pore structure, anisotropy, thermal conductivity, and mechanical performance. Highly anisotropic foams/aerogels can be, for example, prepared *via* unidirectional freeze-casting methods.[106–108] Hybrid foams and aerogels have shown great potential in fields such as engineering, construction,[109,110] energy,[111] and biomedical,[112] and can be applied with different kinds of compounds to design materials with distinct functional properties (Fig. 3).

Additive manufacturing, commonly known as 3D printing, is a technique that enables 3-dimensional customer-specific products with high complexity in design and architecture to be obtained, which are fabricated layer-by-layer using digital designing tools. Thermoplastics are the base of standard 3D printing for polymers (*via* fused deposition modeling) but the use of cellulosic materials as primary building blocks is receiving increasing attention also in 3D printing, simply due to the growing interest in developing fully bio-based materials. Though multiple 3D printing methods have been reported for nanocellulose-based materials,[113] direct-ink-writing (DIW) is the most prominent technique for nanocellulose in the absence of a polymer matrix.[114] In DIW, a liquid phase with low but sufficient viscosity and shear-thinning behavior (to avoid nozzle clogging) is required, as well as a crosslinking mechanism to maintain the printed shape.[115] One of the main uses of DIW is in biomedicine, where the building materials, such as NC, are mixed with cells to create tissue-like structures (referred to as 3D-bioprinting).[114] 3D-bioprinting is revolutionizing tissue engineering considering the requirement for ultra-high rates of reliability in order to precisely mimic the complex architectures that compose the human body. In this context, NC is an excellent candidate as a building block considering its structural similarity to extracellular matrices (ECMs) in terms of porosity and interconnected framework, and excellent biocompatibility.[116]

Moreover, a revolutionizing development in this subject is 4D bio-printing, which incorporates the fourth dimension of "time" to create tissue that responds to a predetermined stimulus, promoting physiologically relevant transformations over time. This is especially important, considering the lack of physico-spatial control of 3D-bioprinting, which is indeed essential due to the dynamic conformational changes of human tissue. Nevertheless, there are still important hurdles in the bioprinting of long-term compatible artificial tissue, such as that (i) the bio-structures should exhibit fast and selective stimuli-responsiveness, (ii) biological tissue adopts anisotropic structures which play a critical role in shape changes and movements in biological organisms, while most current bio-printing approaches use isotropic synthetic polymers, (iii) most crosslinking mechanisms (required to achieve high printing-resolution) rely on chemistries that have off-target biological activity, and (iv) the bio-structures should allow cell-adhesion in a specific manner to ensure full compatibility. To date, no single material has been able to simultaneously address these challenges. Can nanocellulose be the platform to make the perfect material for bioprinting? Can hybridization improve the properties for this purpose? These are still open questions, and it's not something that we will go into in detail within this review article. However, this is indeed something to mention as an outlook of NC-based hybrid materials.

5. Probing the mineralization of nanocellulose *via* advanced characterization tools

The characterization of the nanocellulose hybridization is based on either studying the structural and/or interaction changes in the cellulose material, or aiming for a selective application.[117,118] In this part of the article, our focus is to answer the question of how to elucidate the changes in the nanocellulose structure and properties upon hybridization, specifically focusing on *in situ* processes, where inorganic nanomaterials are grown in nanocellulose matrices, providing insights to the reader about the utilization of techniques which can be used to probe *in situ* hybridizations. The section does not provide the details of the techniques (the readers may look into dedicated reviews on the specific techniques for a better idea about the experimental details, *e.g.*, ref. 117, 119, and 120), but instead provides an overview of the capabilities of these techniques.

Most characterization techniques yield images or spectra, which can be refined for obtaining the topographic, geometric, structural, chemical, or physical details of the system. The information provided by the characterization methods can be used to establish important relations such as cause and effect, and structure and property, and provide guidance in making

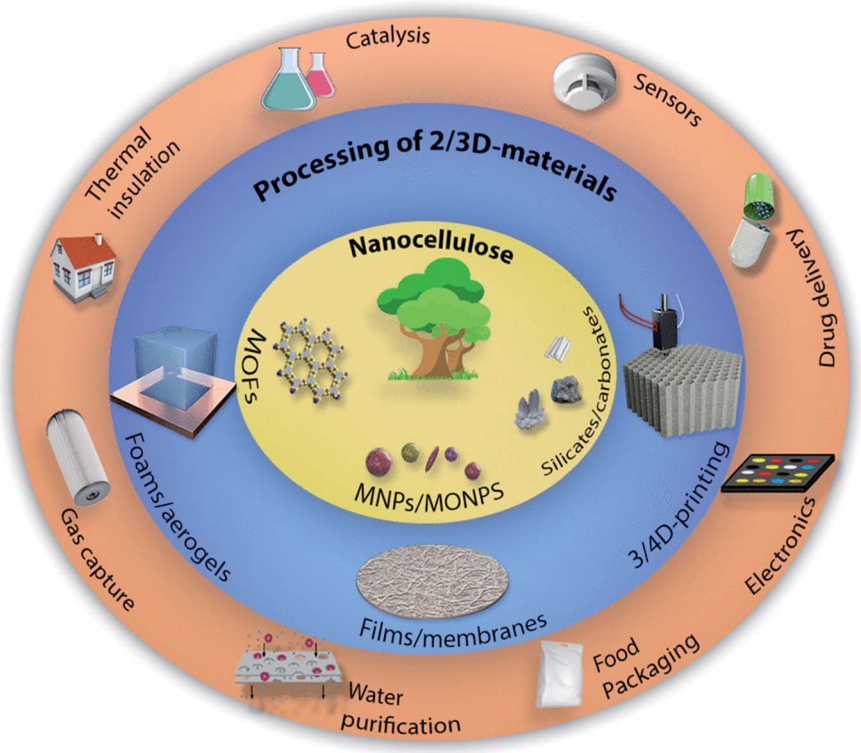

Fig. 3 Conceptual schematic illustration of the subcomponents to hybridize nanocellulose, processing routes, and the potential main applications of the resultant hybrid materials.

critical decisions for their applications. The different characterization techniques used to achieve these objectives can be broadly categorized as spectroscopic, macroscopic, microscopic, and scattering techniques. The spectroscopic techniques (*e.g.*, UV-visible spectroscopy, photoluminescence, infrared absorption, Raman scattering, *etc.*) provide information about chemical compositions, bonding, *etc.* In TEMPO-CNCs hybridized with capped gold nanoparticles, synthesized *in situ* for the detection of pathogenic DNA, the presence of gold nanoparticles has been examined and colorimetric detection of DNA carried out using UV-vis spectroscopy.[121]

The macroscopic techniques such as rheology, zeta potential measurements, TGA, quartz crystal microbalance with dissipation (QCMD), *etc.* provide information on the macroscopic properties of pristine cellulose as well as modifications therein on hybridization. Rheology in combination with several other techniques has been utilized to investigate CNF–silica aerogels prepared by a one-step *in situ* aqueous sol–gel process.[122] In the process, sodium silicate (Na_2SiO_3) underwent hydrolysis and polymerization in the presence of CNFs to yield hydrogels having storage and loss moduli that confirm the ability of CNFs to function as the structural skeleton.[122] Similarly, copper and palladium-oxide nanoparticle loaded CNC-based aerogels have been *in situ* synthesized and characterized by a variety of techniques including macroscopic techniques like BET, porosity measurements, *etc.*[123] QCMD has been used to examine the *in situ* adsorption of the metal ions on the nanocellulose film in terms of adsorbed mass, which is then correlated with the size of the small nanoclusters (Fig. 4(a)).[95]

The microscopic techniques (*e.g.*, scanning electron microscopy (SEM), transmission electron microscopy (TEM), scanning tunneling microscopy (STM), atomic force microscopy (AFM), *etc.*) enable direct visualization of the complex structures in the real space. For instance, the morphology of a hybrid film comprising CNFs mineralized with silver nanoparticles and reduced graphene oxide has been explored using different microscopic techniques.[124] The scattering techniques (*e.g.*, small-angle scattering, diffraction, light scattering, *etc.*) on the other hand provide information on the reciprocal space and are powerful tools for probing the systems in the native state, and in real time. A set of very interesting experiments combining shear-free mixing with scanning *in situ* SAXS have been performed by T. Rosén *et al.*, to obtain time-resolved nanoscale kinetics during the *ion-induced* assembly of dispersed cellulose nanofibrils.[125]

In general, a combination of techniques is required to correctly explore and implement a system, particularly a multi-component system such as NC-based hybrids, in the sense that changes at various length and time scales can be simultaneously investigated by coupling the different techniques. For instance, a recent review article summarizes the coupling of the rheology with the different optical, scattering, and spectroscopic techniques, which are powerful alternatives to study the mineralization of NC-based materials.[126]

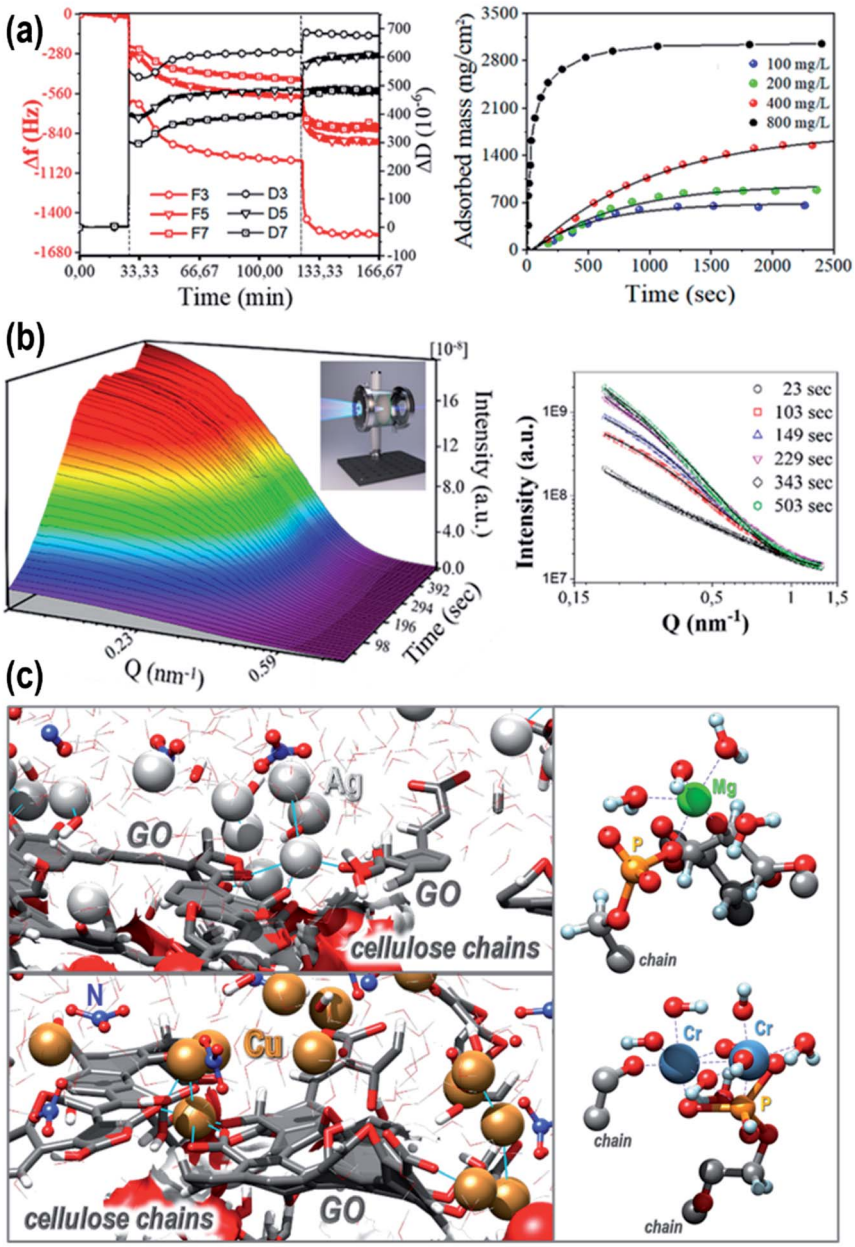

Fig. 4 Selected examples probing the *in situ* hybridization of the nanocellulose (a) utilization of the QCMD to observe the real time adsorption of the metal ion (in terms of adsorbed mass) on the TEMPO-oxidized nanocellulose film.[49] (b) *In situ* SAXS to follow the real-time growth of the nanoparticles on nanocellulose.[49] (c) Various types of metal ions adsorbed on cellulose and GO sheets. The capturing action of the phosphate group towards Mg and Cr ions is shown on the right (fragments extracted from the complex structures). The tendency of the metal ions to self-interact and form clusters is highlighted in the pictures on the left, where copper and silver ions are in contact with the GO sheets sometimes bound to their carboxyl groups.[310]

One of the most suitable techniques for structural *in situ* characterization is small-angle scattering (SAS), as the dimensions of both the components are in nanometer length scales. SAS is a powerful technique that probes nanomaterials to determine their shape, size, and size distribution, the interaction between the particles, and the morphology of their hybrids. In SAS, one measures the intensity of the scattered X-rays/neutrons at low angles, sensitive to the length scales in the nanometer region.[119,127] The structural details of the hybrids based on borate-functionalized cellulose nanofibers and noble-metal nanoparticles have been probed by utilizing SAXS studies. It has been shown that there is a coexistence of the individual nanoparticles and some nanoparticle aggregates in the cellulose matrix. The study utilizes a laboratory-based SAXS instrument and could successfully provide evidence of the formation of the nanoparticles in the hybrid but does not provide kinetics of the growth.[128] In another study, the real-time growth of metal oxide nanoparticles has been followed in the matrix of

nanocellulose (Fig. 4(b)). A vacuum filtration technique has been used for this purpose, where the vapor of the salt solution is passed through the CNF film. The salt ions are found to be reduced in the cellulose film, transformed into nanoparticles, and finally stabilized by the cellulose. These measurements were performed at a synchrotron source and may not be possible at a low-intensity lab X-ray source.[49]

The additional advantage of contrast variation in such two-component hybrids is brought by the small-angle neutron scattering (SANS) where one of the components can be matched to the solvent to examine the structural details of the other. The ease of contrast variation in SANS arises from the difference in the scattering length of the neutron for different isotopes (*e.g.*, the coherent scattering length of neutrons for hydrogen is about −3.74 fm while that for deuterium is about 6.674 fm). Therefore, in a multi-component system, the scattering from one of the components can be suppressed by partial deuteration of either the component or the solvent. The hybrids of the gold nanorods and cellulose nanocrystals have been probed by contrast-matching both the components to the solvent (mixed H_2O/D_2O solvent) one by one, enabling the structural changes in the other to be probed. It has been seen that there is a transfer of the nematic structure of CNCs to gold nanorods, understood by an entropy-driven transition from an isotropic to a cholesteric phase.[129]

QCMD is another technique capable of investigating the *in situ* hybridization of cellulose by different organic/inorganic components. For example, the adsorption of the nanoparticle from a dispersion on a CNF substrate has been probed using QCMD along with AFM imaging.[130] AFM provides direct evidence of nanoparticle adsorption, while QCMD can provide real-time data of the nanoparticles' adsorption in terms of adsorbed mass, uniformity of the layer, *etc.* QCMD is a nano-mechanical acoustic-based technique that utilizes acoustic waves generated by oscillating a piezoelectric quartz crystal sensor and can *in situ* detect extremely small changes (of the order of ng cm^{-2}) in the mass adsorbed on the sensor. The AC field is applied through the electrodes, to excite the quartz sensor, undergoing mechanical shear oscillations, at the resonance and overtone frequencies. Any change in the mass of the sensor through adsorption of the external molecules produces the corresponding changes in the frequencies and dissipation. In the simple case of the uniform layer formation, the changes in the frequency can be directly related to the adsorbed mass, according to the Sauerbrey equation. The dissipation factor ($D_n = 2\Gamma_n/f_n$) is another important parameter, measured in a QCMD, and is related to the dissipative energy losses, caused by the deposited masses. The variation in the dissipation factor can be useful to extract information about the structural changes, in the case when the deposited mass does not form a rigid and uniform film. A low dissipation value suggests the formation of a thin film with rigid properties while a high value indicates the formation of a swollen and mobile film. QCMD data can be modeled to extract the exact morphology of the adsorbed layer. QCMD, being a simple and high-resolution mass sensing technique, is now extensively utilized to study the adsorption of various nanomaterials on the cellulosic surface, reaction kinetics, and degree of hydration. The real-time adsorption of salt ions on the nanocellulose surface has been explored and connected with the formation of nano-clusters of size about 2–5 nm (Fig. 4(a)).[49] In a similar study, the film of regenerated cellulose deposited on the QCMD sensor was exposed to $AgNO_3$ solution to look for the formation of silver nanoparticles.[131]

Innovative utilization of the routine techniques and reconstruction of the three-dimensional images is also one of the most popular recent interests. In a study by Kim *et al.*, hybridization of bacterial cellulose with graphene oxide nanoflakes has been examined for 3D neuronal bilayer formation. The three-dimensional alignment of the CNFs in the hybridized hydrogel, where the 3D stacked images of nanofibers were reconstructed by employing laser scanning confocal scattering microscopy, collected the light scattered at the refractive-mismatched interfaces.[132] Synchrotron-based X-ray tomographic microscopy has also been utilized to create a three-dimensional structure of hybrid aerogels prepared from a scaffold of cellulose and silica sol. The study utilizes phase mapping to extract maximum information including sub-micron topological details of the cellulosic network, affecting the physical properties of the aerogel. Overall, the applicability of synchrotron X-ray tomography has been demonstrated for qualitative and quantitative investigations of complex nanostructures, useful for understanding their macroscopic behavior.[133]

In brief, there are advanced techniques (SAS, QCMD, tomography, *etc.*) that can follow the *in situ* growth of the nanohybrids, which can be utilized to develop a feedback mechanism during the fabrication of these hybrids, enabling control over the process parameters. It is perhaps not possible to describe all the techniques which have been routinely used to probe nanocellulose hybrids, therefore a table summarizing the suitability/applicability, advantages, and limitations of these techniques as well as selected examples has been presented in the ESI (Table S1†).

Computer simulations are also of great importance in understanding the formation of NC-based hybrids, at the microscopic as well as macroscopic level, and help to establish structure–property relations. Through modeling, one can handle molecular models made of thousands of atoms and explore their evolution for extended periods (tens of nanoseconds and many thousands of configurations). However, modeling mineralization reactions is not an easy task (especially for biopolymers with complex structures such as NC) as the current simulation methods have important limitations. For instance, molecular models are often limited to crystalline forms and selected portions of the cellulose chains, resorting to periodic boundary conditions to mimic an infinite size. The systems are typically described either at the atomic or at the granular level (coarse-grained models), where groups of atoms are condensed into representative beads. These simplifications result in modeling of the macroscopic behavior, such as the determination of amorphous transition states for the room-temperature conversion of the cellulose allomorphs and characterization of the interface between the crystalline forms of these structures;[134] the reproduction of the partitioning free

energies between water and other solvents including, sometimes, "*ad hoc*" cellulose–cellulose nonbonding interactions;[135] the evaluation of the effects due to solvents on the transition from crystalline to amorphous structures;[136] the analysis of different physicochemical and mechanical properties of native cellulose fibers and the physical response to temperature and mechanical bending;[137] the description of the fibril orientations and motion upon cellulose deformation,[138] *etc.* However, a more meticulous inspection of each part of the system, with an atomic-level representation that possibly includes reactivity (bond breaking and formation), is crucial to simulate an *in situ* hybridization process, where chemical reactions occur (typically ions with hydroxyl/carbonyl groups in cellulose), proceeded by the formation of nanoclusters and subsequent aggregation to form the resultant nanoparticles.

The option to include reactivity in classical molecular dynamics simulations of materials is offered by a few potentials,[139–143] and it has been elegantly and efficiently improved, and expanded in the ReaxFF paradigm,[144] which has been extended over the years to many different branches of materials science.[145] As far as cellulose is concerned, recent ReaxFF MD simulations have shown the behavior of cellulose at high temperature,[146–149] and its decomposition, dehydration, and evolution in the geological context. ReaxFF has also been used to study the influence of metal ions on cellulose behavior, recognizing major intrafibrillar rearrangements at the fibril surface and not involving the core.[45] A relevant study was done by Zhu *et al.*, who used the ReaxFF MD methodologies to study the assembly of nanocellulose and graphene oxide,[150] disclosing the formation of layered cellulose–graphene oxide configurations, molecular networks, and the decisive cooperative action of all the assembled components. They prepared a great variety of different multi-component models, containing many thousands of atoms to evaluate the synergy of cellulose and GO, and to estimate the fiber packing, and material porosity. Through this, the authors extracted representative configurations from the last 50–100 ps of the production molecular dynamics (MD) trajectories, and an accurate analysis was carried out. Distance and spatial distribution functions, root mean square deviations of the cellulose atoms in relation to average reference structures, hydrogen bonding networks, percentage of adsorbed ions, protonation states of the side chains, intermolecular interactions, and other useful information related to the solvent effect, such as water penetration and diffusion inside the cellulose matrices, ion solvation layers, *etc.*, were examined in detail.

Zhu and collaborators also found that GO sheets of various sizes could self-interact both in solution and inside the cellulose material, forming nanoparticles *in situ*. As experimentally noted, the GO sheets could lay flat on the surfaces of the fibers and, as theoretically observed, be stably anchored to cellulose layers through intermolecular hydrogen bonds between their hydroxyl/carboxyl groups and the respective cellulose moieties, which were sometimes reinforced with the connections of the functionalities of the GO primary planes.

All the presented models of a cellulose-based material, where pristine cellulose was engineered (adding GO sheets, functionalizing the side chains with carboxyl, phosphate, and methyl groups, *etc.*), were fruitfully used to disclose possible mechanisms of the entrapment of various types of metal ions (such as Cu^{2+}, Ag^{+}, Ca^{2+}, Zn^{2+}, Mg^{2+}, Cr^{3+}, *etc.*), and their cluster formation. The adsorption and capture processes were analyzed following the trajectories of the ions from the solvent to the material interface, focusing on distance distributions of the neighboring species and types of interactions. As far as copper is concerned, the simulations showed that, in solution, it was usually found in various types of complexes with the surrounding water oxygens, namely distorted tetragonal, octahedral, square pyramidal, and trigonal bipyramidal configurations, with an average Cu–O distance of approximately 2.0 Å, but also in combination with its charge balancing counterions. The presence of a negatively charged material acted as an attractor that could drive the ions and induce their migration towards specific locations. In the case of cellulose, the preferential landing regions were those where a charge balance was reached. There, the ions were stably anchored to the interface through the cooperative interactions of the main attractors (carboxyl) and the hydroxyl of all the composite components (concerted action), as suggested by the first peaks at 1.8–2.0 Å of the distance distribution plots. Furthermore, depending on the ion concentration, the adsorbed ions showed the tendency to form metal clusters at the material interface, probably because their complexation/immobilization created nucleation seeds for nanoparticle growth, thus being one of the first simulations to indicate a mineralization reaction in an NC-based material, corroborating experimental results, thus suggesting the great potential of using computation simulations for disclosing mineralization processes, making it a prominent research subject to investigate further with different subcomponents, and in different environments. A few examples of ion trapping mechanisms are shown in Fig. 4(c).

6. Applications of nanocellulose-based hybrid materials

The *in situ* growth of a secondary component can be performed on the reactive surface of nanocellulose, which bears a vast amount of functional groups (mainly hydroxyl) to do so. Nature has been mineralizing biopolymers from the beginning of life to create complex structures. Besides the inorganic matter (*e.g.*, calcium carbonate) which has been mineralized by nature from the beginning of life, more functional nanoparticles (*e.g.*, MOFs, M(O)NPs, *etc.*) can be *in situ* grown to introduce properties that synergistically complement the already outstanding properties of NC. The acquired properties of nanocellulose can be utilized, upon processing onto 2/3D materials, in applications such as (i) separation applications (gas separation/water purification), (ii) biomedical applications, (iii) energy applications, *etc.*

6.1. Hybrid materials for separation applications

For gas separation. Due to the alarming rate at which the concentration of carbon dioxide (CO_2) is increasing in the atmosphere and its influence on the current global climate

change,[151] there is a critical need to develop new technologies to reduce industrial CO_2 emissions. Carbon Capture and Storage (CCS) and Utilization (CCU) technologies contribute *via* solutions to reduce industrial and farm CO_2 emissions.[152] These technologies must be inexpensive while following the principles of sustainability. Porous sorbent materials such as zeolites[153] and MOFs[70,154,155] have stepped up to ameliorate this problem. Nevertheless, there are still several challenges to solve before their large-scale utilization, such as their poor processability into desired shapes considering that they are in a powdered state and that the use of binders normally leads to micropore blockage.

Currently, the combination of sorbent materials (*e.g.*, MOFs) and NC upon mineralization is being sought, due to the great versatility that NC offers as a support material and processability into 2/3-dimensional materials. The high surface area of NC favours the formation of highly porous structures with high loadings of mineralized sorbent material.[12,156] Such hybrid structures are gaining attention as gas sensors and barriers, as well as biogas upgrading materials due to their flexibility, biodegradability, and bio-based nature. See Fig. 5 for some examples of mineralized NC structures with MOFs.

The use of 3D structured bio-based foams, which can act as support sorbent materials, appears to be a key alternative towards the industrial implementation of sorbents for CO_2 capture. For instance, Valencia *et al.* formulated a series of ZIF-L/gelatin/TOCNF by the *in situ* synthesis of ZIF-L on TOCNF physically crosslinked with gelatin and freeze-drying foaming. The CO_2 adsorption–desorption was measured by a volumetric gas method at 298 K and 1 bar exhibiting a direct correlation between ZIF-L content, surface area, and CO_2 capacity. The foam with a density of 37.4 kg m^{-3} and surface area of 10 m^2 g^{-1} exhibits a superior adsorption capacity (ZIF-L 50 wt%/gelatin/TOCNF hybrid with 0.75 mmol g^{-1}).[157] The shape of the CO_2 adsorption isotherm of pure ZIF-L and the ZIF-L 50 wt%/gelatin/TOCNF hybrid is similar and less steep at low pressures compared with NaA zeolite ones.[158] The shape of the isotherm indicates a degree of chemisorption, which means an irreversible CO_2 uptake, which was confirmed during the first and second cycles of the breakthrough experiments performed by thermogravimetric analysis.[159] It is known that a chemical interaction occurs between CO_2 and positively charged ZIF-L, *i.e.*, free imidazole linkers,[155] that may need an input of thermal energy to break similar to that used in the temperature swing adsorption (TSA) processes. However, TSA processes may destroy the cellulosic foams, so vacuum and pressure adsorption (VSA and PSA) processes are ideal for these hybrid foams.

Apart from the CO_2 uptake capacity at 1 bar, the swing adsorption capacity must be calculated for the selection of the best adsorbent. The CO_2 swing adsorption capacity is estimated as the difference between the CO_2 uptakes at 1 bar and 0.15 bar, representative of a PSA cycle. The CO_2 swing adsorption capacity, also known as the working capacity, of pure ZIF-L at 0.15 bar is about 0.5 mmol g^{-1}, half of that obtained for NaA zeolites.[158] The estimated CO_2 working capacity of the ZIF-L/gelatin/TOCNF hybrid may seem good for PSA processes as the ZIF-L content increases.

The third important adsorbent feature is ideal CO_2/N_2 selectivity which is related to the purity of the exhaust gas. Valencia *et al.* reported the apparent selectivity using Henry's law from the weight change of single-component sorption experiments by thermogravimetric analyses where the

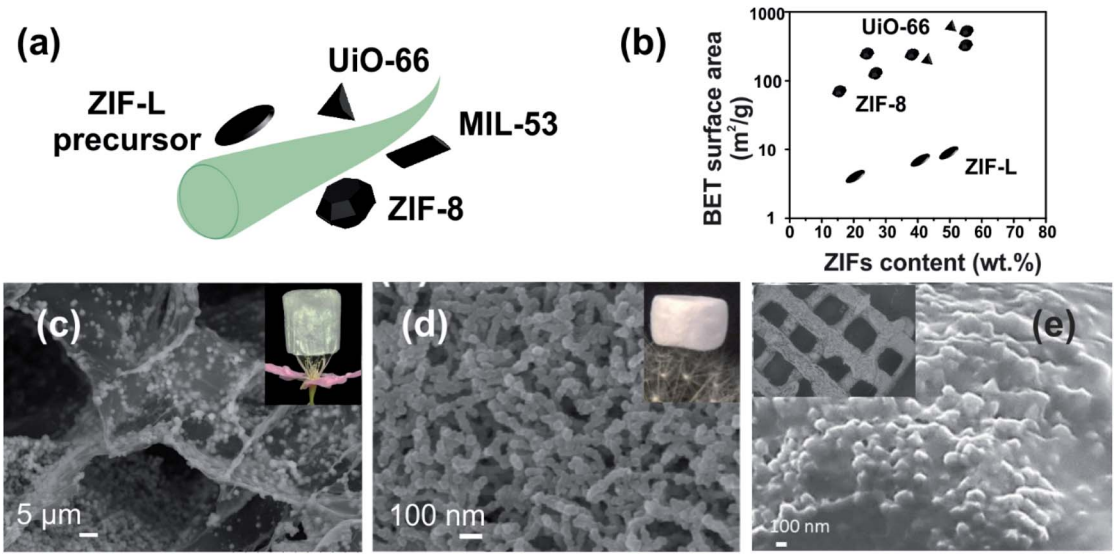

Fig. 5 MOF/nanocellulose aerogels for gas adsorption. (a and b) Illustration of CNFs loaded with Zn-, Al-, and Zr-MOF crystallites (ZIF-L[47] or ZIF-8,[46,75,89] MIL-53,[80] and UiO-66,[93] respectively) as promising hybrids for gas adsorption based on their high BET surface area. SEM images showing well distributed (c) ZIF-L[47] and (d) ZIF-8 (ref. 91) on nanocellulose sheets and fibers, while the insets in (c) and (d) depict the light weight of the foams by resting on the top of flowers. Only (c) ZIF-L/TOCNF "MF-3" has been tested for CO_2 adsorption (0.75 mmol g^{-1} at 298 K and 1 bar)[47] so far. From the same laboratory a promising (e) 3D printed monolith CO_2 adsorbent "CelloZIF8"[45] prepared using alginate, ZIF-8, and TOCNF shows a super-high surface area (2330 m^2 g^{-1}).

hypothetical flue gas mix was 50% : 50% CO_2 : N_2.[157] 50 wt% ZIF-L gelatin/TOCNF foam presented the highest selectivity (CO_2/N_2 = 11) among the hybrids tested, a value that is comparable to zeolitic sorbents. We highlight that, although there is a comprehensive review of CO_2 adsorption and kinetic models in aerogels by Keshavarz *et al.*[160] and on the thermodynamics of CO_2 adsorption by Anas *et al.*,[161] there is a lack of information about the gas sorption performance of bio-based aerogel hybrids,[162] for instance, the ones composed of cellulose and MONPs, MOFs, and other microporous polymers with nanometric dimensions.

Regarding 2D structured hybrids as CO_2 sorbents, Chao *et al.* proposed several MOF/CNF nanohybrids (ZIF-CO3-1/CNF, Al-MIL-53/CNF, ZnMOF-74/CNF, and HKUST-1/CNF) with an average surface area of 94, 2019, 246, and 281 $m^2\ g^{-1}$, respectively, that would be viable membranes for gas adsorption.[163] Later the author demonstrated the CO_2 capacity of ZIF-8/CNF membranes prepared by the same method. Briefly, the CNFs (TEMPO-oxidized CNFs) were first modified by ion-exchange using an excess of the corresponding metal and polyvinylpyrrolidone (PVP). This ensures the crosslinking of CNFs. The crosslinked CNF and MOF precursors were mixed at 298 K for 1 h before the vacuum filtration and pressing to generate membranes with 25 wt% MOF loadings. The surface area of the ZIF-67/CNF hybrid was exceptionally high (687 $m^2\ g^{-1}$) *versus* the 325 $m^2\ g^{-1}$ for ZIF-8/CNF. Only the latter was tested for CO_2 and N_2 adsorption at 293 K and 1 bar. The high slope of the CO_2 adsorption isotherm suggests irreversible chemisorption on the ZIF-8/CNF membrane at very low pressures which may be an issue for the PSA processes. The CO_2/N_2 selectivity was calculated using Henry's law from the initial slopes of the single-component isotherms obtained from the volumetric analysis. The flexible membranes showed optical transparency and CO_2/N_2 selectivity of 6 with 25 to 50 wt% ZIF-8 loadings.[164]

In the studies of Yao *et al.*, a series of membranes of cellulose nanofibrils with added Zn and Ca cations,[165] Zn-ZIF (ZIF-8),[166] and amine-modified Zr-ZIF (UiO-66-NH_2)[167] were developed for CO_2 separation. For instance, Jia *et al.* prepared ZIF-8 with TOCNF using different concentrations of MOF salt (10–90 wt%). The highest CO_2 permeability (550 barrer) and CO_2/N_2 selectivity equal to 46 was achieved by the ZIF-8/CNF hybrid containing an actual loading of 33 wt% (corresponding to sample ZIF-8/CNF-70).[166] The reusability of the membrane over 48 h confirmed the stability for CO_2 permeability at room temperature (298 K) and 3 bar. Besides, the increase of the ZIF-8 content produces a rough membrane with undesirable nanoparticle agglomeration. The authors were able to increase the CO_2 permeability by two times at 358 K with consequent destruction of the cellulosic membrane underlining the importance of the working temperature.[168]

The same group explored the amine modification of Zr-ZIFs like University of Oslo-66 (UiO-66), known for its high surface area of 737 $m^2\ g^{-1}$, to be encapsulated on cellulose layers. *In situ* synthesis of UiO-66-NH_2 on diluted solutions of CNFs avoids nanoparticle agglomeration. Moreover, the insertion of amino groups using amino terephthalic acid allows the crosslinking with TCNF. Although the surface area of UiO-66-NH_2/CNF hybrids was not determined, it shows a clear improvement of the CO_2 permeability. The free primary amines over sorbent nanoparticles enhanced the permeability of CO_2 (139 barrer) and CO_2/N_2 selectivity (46) at 298 K and 2 bar possibly due to the chemisorption as previously explained.[167] The same approach was tested on Al-MIL-53 using *N*-methylpyrrolidone by Mubashir *et al.*[169] The 2D structures were prepared by a solution blending method in which previously synthesized MIL-53 particles with a BET surface area of 637 $m^2\ g^{-1}$ were added to cellulose acetate (CA) solution and cast. The cellulose solution prevented the agglomeration of MIL-53 by acting as a capping agent and tripled the CO_2 selectivity of its hybrids. A CO_2 permeability of 53 barrer and CO_2/N_2 selectivity of 23 at 298 K and 3 bar were obtained by the NH_2-MIL-53/CA hybrid with 15% loading. Interestingly the hybrid was resistant to plasticization when tested at high pressure (30 bar). Whether the 2D structures, membranes, or films are prepared by vacuum filtration, solvent casting, or dip coating, the problem of the industrial-scale synthesis still arises, even though their performance is fairly close to Roberson's 2008 upper bound for CO_2 permeability and CO_2/N_2 selectivity.[170] Table S1† shows a general comparison of the gas absorption performance of nanocellulose hybrids in 3D and 2D architectures.

The limited access to characterization equipment like ASAP, GEMINI, or the like for testing CO_2 sorption properties is a drawback for measuring the separation gas capacity and performing the optimization of already promising 2D and 3D hybrids, and we often see such new adsorbents tested for decontamination. However, the reported specific surface area through N_2 adsorption at 77 K and the Brunauer–Emmett–Teller (BET) method on dry specimens does reveal the potential gas uptake capacity of nanocellulose hybrids. The BET method measures the amount of sorbate in a monolayer (often multilayer) of the surface of the sorbent, therefore determining the available surface area for other molecules to interact with. However, the routinary sample drying and degassing before gas sorption measurements often causes the 3D network to collapse[160,168] and probably promotes the formation of hydrogen and lactone bridges due to the Lewis acid sites in MOF/nanocellulose hybrids.[171] Even though the BET method often underestimates the surface area on cellulosic materials it is a recurrent parameter in the CCU and CCS literature. The estimation of the surface area on non-dry samples could be more relevant for biogas upgrading in nanocellulose hybrids since humidity contributes to CO_2 adsorption on amine-modified surfaces. Chemical methods, for instance, sodium hydroxide titration, specific xyloglucan adsorption, and the Ougiya method on non-dry nanocellulose samples should provide a more realistic measurement of the surface area on nanocellulose hybrids.[171–173] Beyond their advantages and disadvantages, those specific surface area determinations allow the screening of the best candidates to perform gas adsorption and here we did an exercise by reviewing promising 3D MONPs (and MOFs)/nanocellulose hybrids.

MONPs like ZnO are recognized by strongly interacting with CO_2 through the formation of bicarbonate, carbonate, and carboxylated species, and recently by their role as photocatalysts

in the CO_2 transformation into fuels like methane, methanol, and ethanol.[174,175] Soltani *et al.* reported a ZnO/NC hybrid with a higher specific surface area (295 $m^2 g^{-1}$) than that of zeolite/TOCNF with demonstrated CO_2 uptake capacity (200 $m^2 g^{-1}$ with CO_2 adsorption of 1.2 mmol g^{-1}).[173,176] The promising 2D ZnO/NC hybrid was prepared by solvent evaporation and *in situ* formation of ZnO nanoparticles using diluted TEMPO-oxidized CNFs. The CNFs were obtained from a local source of waste cooler straw which promotes synthetic approaches that resonate with circular economy principles.

Among the high surface area 3D foams containing MOFs, we found that those composed of Zn-, Al-, Fe-, and Zr-ZIFs (ZIF-8, MIL-53, MIL-100, and UiO-66, respectively) are commonly found in the field of water remediation, again due to the elaborateness and often expensiveness of gas sorption studies. Today, the maximum MOF loadings on foams reach 50 wt% before the collapse of the 3D structure, and the challenge is to increase the MOF dispersion and/or reduce the particle size. Several reported preparation approaches aim for dispersion and size reduction which eventually increases those loadings, improves the surface area, and boosts gas adsorption capacity. A two-step approach in which ZIFs are firstly formed allows both high loadings and surface area in the nanocellulose hybrids. For instance, Nie *et al.* prepared ZIF-8/CNF/cellulose membranes (308 $m^2 g^{-1}$) and foams (475.5 $m^2 g^{-1}$) with a high BET-specific surface area.[177,178] The preparation of ZIF-8/CNF/cellulose foams consisted of two steps: (1) synthesis of well-formed dodecahedral ZIF-8 nanoparticles over a cellulose suspension by hydrothermal treatment at 348 K for 24 h and (2) homogenization with CNFs before the freeze-drying foaming. Interestingly, the surface area increased with both CNF and ZIF-8 loadings from 80 $m^2 g^{-1}$ for ZIF-8 (16%)/CNF (10 wt%)/cellulose up to 475 $m^2 g^{-1}$ for ZIF-8 (55.2%)/CNF (40 wt%)/cellulose.[177] Meanwhile, Ma *et al.* reported ZIF-8 (55 wt%)/bacterial cellulose (BC) hybrids using a two-step synthesis to produce foams. The procedure consists of (1) pre-forming a BC aerogel *via* the freeze-drying method and (2) dispersion of Zn-ZIF precursors over aerogel until full swelling and low-temperature crystallization at 298 K for 2 h under sonication. The specific surface area of ZIF-8 (55 wt%)/BC foams (636 $m^2 g^{-1}$) was still below that obtained in the pure ZIF-8 (956 $m^2 g^{-1}$)[179] but high enough for a gas adsorbent. Zhu *et al.* reported a three-step synthesis that produced a ZIF-8 (81 wt%)/CNF foam with a surface area of 890 $m^2 g^{-1}$ which is one of the highest loadings and surface areas found in the literature.[180] Similar results were reported by Su *et al.* for ZIF-8 (90 wt%)/CFs with a surface area of 620 $m^2 g^{-1}$.[181] The preparation consisted of (1) dispersion of Zn-ZIFs precursors and CNF suspensions for 24 h, (2) crystallization of MOF at 298 K for 12 h, and (3) foaming by the freeze-drying method. The *in situ* synthesis of ZIF-8 nanoparticles forms 3D structures made up of bead-like strings. The differences in the synthetic procedures demonstrate that a good dispersion of nanoparticles is key to increasing the mineral content (*i.e.*, ZIF loading) and doubling the surface area.

Other Zr-ZIFs like UiO-66 nanoparticles pre-synthesized and loaded on NC suspensions were used to prepare foams by freeze-drying. These UiO-66/NC hybrids show a higher BET surface area (826 $m^2 g^{-1}$) than those synthesized *in situ* over nanofibers (*i.e.*, 267 $m^2 g^{-1}$).[179,182,183] This synthetic approach allows high loadings (*i.e.*, 55 wt%) on the foams, but also spun fibers can even support high amounts of mineralized materials with a less brittle and fragile appearance. Chen *et al.* tested the concept by loading 72 wt% UiO-66 on cellulose acetate fibers fabricated at laboratory and pilot scales reaching a BET surface area of 652 $m^2 g^{-1}$.[184] Similar results were obtained for Al-ZIFs (MIL-53)/CA and NaY/CA hybrids (334 and 598 $m^2 g^{-1}$, respectively).

6.2. Hybrid materials for water purification

With the great industrialization and overpopulation in modern society, humans tend to contaminate the Earth's water streams with hazardous substances such as heavy metals, microplastics, pharmaceuticals, pesticides and herbicides, dyes, and other organic and inorganic compounds.[185] Nanocellulose has been extensively studied for water treatment applications,[185–187] where the most common structures for water filtration systems are two-dimensional such as porous membranes and films, and the properties can easily be tuned by calibrating the aspect ratio of the fibrils, or carefully controlling the processing method (as different filtration times, pressures, or drying yields different morphologies and architectures of the films) and thus variable flux and removal capacity.[188] Nanocellulose by itself can physically adsorb pollutants *via* electrostatic interaction with the anionic groups in its structure (–OH, $–OSO_3$ or $–COO^-$), and conventional surface treatments of nanocellulose can increase the adsorption capacity, due to the introduction of a greater amount of anionic groups (for instance *via* TEMPO-mediated oxidation, which selectively introduces carbonyl groups leading to a nanomaterial with good adsorption capacity of heavy metal ions and dyes[189]).

An alternative way to further improve the adsorption capacity of nanocellulosic materials is *via* hybridization, for instance upon mineralization of MONPs. Water treatment using MONPs, such as Cu_2O, ZnO, or Fe_2O_3, is essentially through photocatalytic degradation of organic and inorganic pollutants, which is an eco-friendly and cost-effective method. The photocatalysis for these semiconductor nanoparticles involves (i) the generation of electrons in the conduction band and holes in the valence band pairs upon light irradiation (with light irradiation greater than the semiconductor band gap); (ii) the migration of the electrons and holes to the surface of the semiconductor, and (iii) the oxidation of water molecules to produce hydroxyl radicals ($^{\bullet}OH$) and reduction of dissolved oxygen to form superoxide radical anions ($^{\bullet}O_2^-$). The formation of these radicals, having higher oxidation potential, degrades the organic pollutants mainly into water and carbon dioxide.[190] The role of (nano) cellulose, when combining it with MONPs for water treatment, is mainly as a template for their mineralization. The growth of MONPs has been extensively studied, mainly under hydrothermal conditions and/or in the presence of a reducing agent. However, Valencia *et al.* have demonstrated that TOCNF can form different MONPs (such as Cu_2O nanoparticles) upon adsorption, at room temperature, and without the addition of

any further reagent. This phenomenon is believed to be due to the presence of both aldehyde and carbonyl groups, the carbonyl coordinating with the ions and therefore increasing the collision probability with the aldehyde groups, which can act as a reducing agent. Valencia *et al.* have shown that the resultant hybrid materials, specifically focusing on Cu_2O/TOCNF hybrids, can be used to form self-standing films for photocatalytic degradation of dyes. Therefore, the materials have triple functionality: the capture of heavy metal ions (*e.g.*, Cu(II)) from water, dye removal, and improved antimicrobial properties. A schematic representation of this approach is shown in Fig. 6.[49]

Several other authors have studied the MONP mineralization on nanocellulose for water treatment. For instance, Lu and collaborators have used a ZnO/NC hybrid material to remove Pb(II) with a maximum capacity of 63.78 mg g^{-1},[191] while Alipour and collaborators have reported a maximum capacity of 554.4 mg g^{-1} (ref. 192) for a similar system. Furthermore, Amiralian and collaborators prepared membranes comprising magnetite nanoparticles grown on CNFs which were used as catalysts for the degradation of rhodamine B (RhB) with peroxymonosulphate (PMS). The results have shown up to 94.9% degradation of RhB after 5 minutes, indicating the successful activation of PMS.[193] Cruz-Tato and collaborators have reported the preparation of an NC-based membrane hybridized with silver and platinum nanoparticles. They prepared membranes with varying pore sizes and tested them with forward osmosis of different solutions such as water, urea, and wastewater. The obtained results show that the membranes have high water flux and solute rejection when tested with wastewater.[194]

Mineralization of NC with MOFs is another well-studied method for water treatment processes. MOFs are highly porous, crystalline materials with excellent potential as adsorbents. Hashem and collaborators reported the preparation of membranes for the removal of metal ions and organic dyes from water. More specifically, UiO-66-NH_2, a zirconium-based MOF, was mineralized on cellulose fibers and processed in membranes. The membranes were tested with simulated wastewater for the adsorption of Cr(VI) and methyl orange, showing a 78.2% and 84.5% removal capacity, respectively.[195]

Two-dimensional systems may dominate the field of water purification when it comes to nanocellulose based materials. However, 3D materials such as foams/sponges can also be produced using (nano)cellulose and used for such applications. Often, chemical crosslinkers, such as glutaraldehyde (GA), maleic anhydride (MA), and polyethyleneimine (PEI), may be used to form a mechanically stable body, as it is not easy to physically crosslink nanocellulose in water-stable 3D structures, but it is not always necessary. Mo and collaborators have reported the preparation of a MOF/TEMPO-oxidized CNF aerogel processed *via* the freeze-casting method. The preparation method provides an abundance of chelating sites for metal

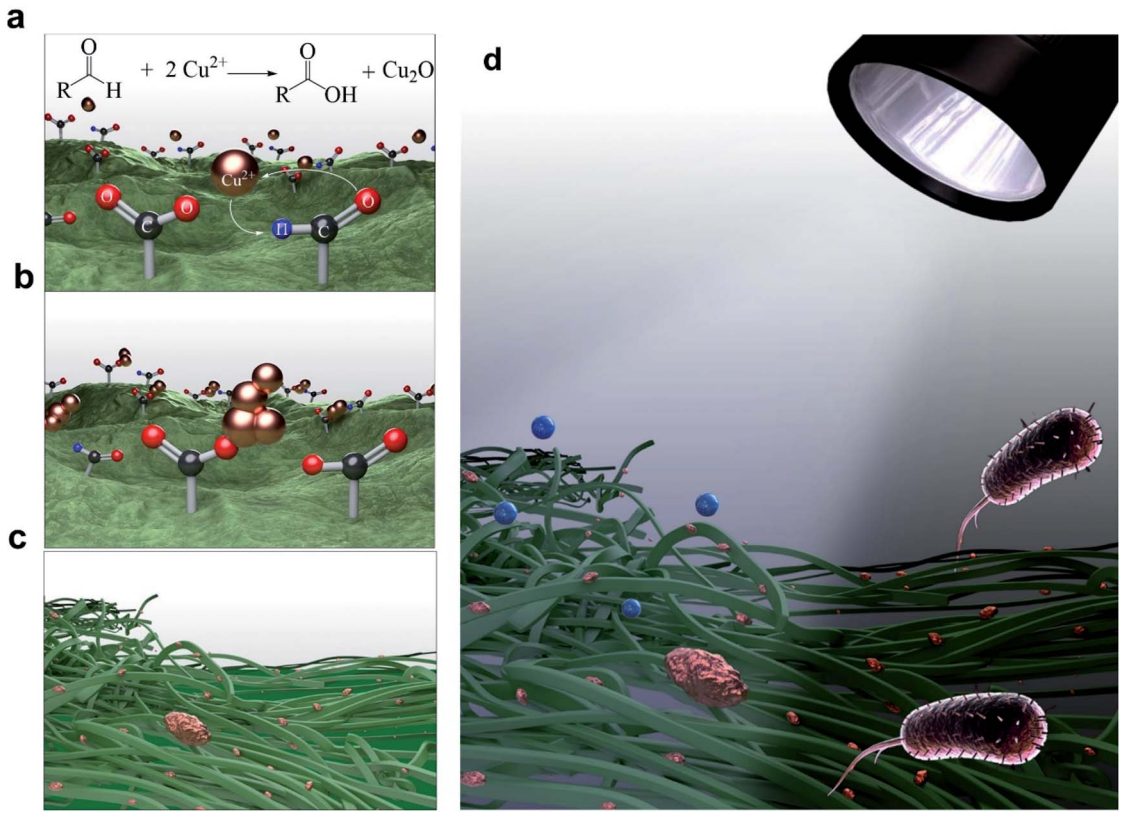

Fig. 6 Mineralization of copper oxide nanoparticles on TOCNF films. (a) Reduction of Cu^{2+} ions to Cu^{+} by the aldehyde groups on TOCNF. (b) Growth of copper oxide nanoclusters. (c) Coalescence of nanoclusters to form Cu_2O nanoparticles. (d) Schematic representation showing the antibacterial/photocatalytic activity of the resultant hybrid membrane.[49]

binding which is reflected in the high uptake capacity tested with Cu^{2+} (300 mg g^{-1}). Moreover, the aerogels have good reusability as there was no dramatic reduction in their adsorption performance after 5 cycles.[196] Similarly, Li and collaborators have recently published a study where TEMPO-oxidized CNFs were decorated with a zirconium-based MOF (*i.e.* UiO-66-EDTA, similar to the one mentioned above) and processed into aerogels using carboxymethyl cellulose as a crosslinker, *via* the directional freezing method. The aerogels show tunable morphologies and characteristics by controlling the composition. Their adsorption performance was tested with water containing Cr^{3+}, Cu^{2+}, Co^{2+}, Ni^{2+}, and Mn^{2+}. An overall removal efficiency of 91% (98% when tested with individual metal solutions) has been obtained, with a reduction only down to 88% after 5 cycles, further illustrating the reusability of the aerogels.[183] NC has also been hybridized with magnetite nanoparticles for the preparation of aerogels with magnetic properties. Gu and collaborators manufactured aerogels composed of oleic acid, NC, and magnetite nanoparticles for the separation of oil and organic solvents from water. The adsorption performance was tested with pump oil, cyclohexane, and ethyl acetate reaching up to 60.50, 68.06, and 60.50 g g^{-1}, respectively.[197]

The mineralization of MONPs on nanocellulose can also be implemented on other 3D materials, such as aerobeads. Crosslinked NC can be shaped into spherical adsorbents by pouring NC suspension dropwise into liquid nitrogen followed by lyophilization.[198–200] The advantages of these systems rely upon the fact that they can be removed, washed, and reused without any special effort. For instance, Mohammed *et al.*[201] produced CNC–alginate hydrogel beads through the intermolecular cross-linking of alginate chains in the presence of Ca^{2+} by dropwise pouring CNCs into a $CaCl_2$ solution. The potential of these nanocellulose based 3D structures as water filtration systems was evaluated with the removal of negatively charged contaminants, for instance, Cu(II), and inorganic dyes, such as methylene blue and Congo red, as well as oil adsorption.[198–203] Moreover, magnetic spherical aerobeads based on nanocellulose and Fe_2O_3 nanoparticles were prepared by Karzar Jedi and collaborators and were tested for the separation of oil and inorganic solvents from water. The hybrid beads have been shown to possess a maximum adsorption capacity of 279 mg g^{-1} for castor oil and up to 100 mg g^{-1} for dimethyl sulfoxide (DMSO). These beads can be easily removed and reused after simple mechanical squeezing, retaining their reusability for at least 10 cycles.[204] Moreover, Gu and coworkers have reported a nanocellulose/magnetic hybrid aerogel and its use for the removal of cyclohexane, ethyl acetate, and pump oil, reporting maximum adsorption capacities of 68.06 g g^{-1}, 56.32 g g^{-1}, and 33.24 g g^{-1}, respectively.[197]

6.3. Hybrids for biomedical applications

Besides the outstanding aforementioned properties of nanocellulose (*e.g.*, excellent mechanical properties, a reactive surface that allows functionalization, processability into porous 2/3D structures, *etc.*), NC also exhibits good biocompatibility and low cytotoxicity, as well as biodegradability which makes it a good candidate for biomedical applications. Nanocellulose alone or hybridized with suitable inorganic (metals, metal–organic-frameworks, *etc.*) and/or organic (drugs, biomolecules) entities have readily shown prominent applications in a variety of medical fields such as drug delivery, wound-healing, implants, tissue engineering, scaffolds, dental grafting, cardiovascular devices, biosensors, *etc.*[205–210] A conceptual schematic representation of the types of biomedical applications for nanocellulose-hybrid materials is shown in Fig. 7.

Beginning with the application of nanocellulose for drug delivery, cellulosic materials (including NC), as approved by the FDA, have been readily accepted for the development of drug reservoirs as well as release platforms. However, native NC possesses almost no antimicrobial properties and limited interaction with certain drugs. In this regard, selectively hybridized NC with different components having antimicrobial activity, as well as better interaction with drugs, are being explored for developing drug delivery systems with superior therapeutic properties. Nanogold/nanocellulose (GNP/NC) hybrids have been utilized for developing transdermal drug delivery, where the gold nanoparticles provide the additional advantage of enhanced skin permeation, required for the transdermal route of drug delivery.[211] This route of drug delivery has several advantages, but the transportation of hydrophilic drugs across the skin is difficult due to the ordered architecture of the stratum corneum (SC). It has been realized that gold nanoparticles can be one of the best-suited materials to disrupt the stratum corneum barrier because of their size in the nanorange as well as their hard shape compared to chemical penetration enhancers. This fact was utilized by the authors to create a novel transdermal device for the administration of diltiazem hydrochloride, based on a polyelectrolyte complex (PEC)

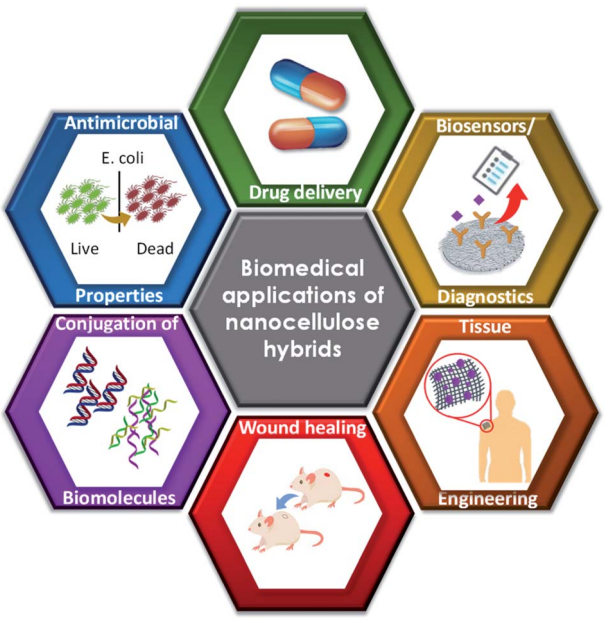

Fig. 7 Schematic representation of the types of biomedical applications for nanocellulose-based hybrid materials.

reinforced with GNP/NC. The GNP/NC was synthesized *via in situ* reduction of the gold salt in the NC matrix. The pharmaceutical applications of the device were investigated by subjecting it to *in vivo* skin adhesion and irritation in humans, cell viability, and environmental fitness studies. The results suggest that the film has enormous potential as a transdermal drug delivery device. Fakhri *et al.*[212–214] developed multiple hybrid materials based on nanocellulose and metal- or metal oxide nanoparticles/quantum dots for application as drug delivery systems. For example, the hybrids of Fe_3O_4–Ag_2O quantum dots decorating CNFs were prepared for the delivery of the cancer drugs etoposide and methotrexate. In this material, CNFs act as a matrix-forming material for long-lasting sustained drug delivery, while drugs are adjoined to the quantum dots. In addition, Ag_2O provides antioxidant, antibacterial, and antiparasitic activity while Fe_3O_4 gives magnetic character. The *in situ* synthesis of ZnS–cellulose hybrids has also been reported for controlled drug delivery applications and antibacterial activity.[215] In another study,[216] a zinc glutamate biological metal–organic framework supported on cellulose fabrics has been utilized for the controlled delivery of nitric oxide (NO) and 5-fluorouracil (5FU) for wound and/or skin cancer therapy.

Nanocellulose has also been extensively utilized for wound dressing applications due to its ability to eliminate exudates, avoid infections and reduce local pain. The major concern in wound healing is the risk of bacterial infection, which restricts the use of pristine cellulose due to almost negligible activity against the infection, as mentioned earlier. However, NC hybrids with metal/metal oxides or metal–organic-framework nanostructures have been emerging as an attractive option for developing wound healing devices, which not only prevents bacterial infection but also promotes angiogenesis, a process involving the growth of healthy cells.[40,217–222] These hybrids, apart from exhibiting the excellent biocompatibility of cellulose also display the antimicrobial capabilities of these inorganic nanostructures. Wu *et al.*[223] *in situ* synthesized silver nanoparticles on CNFs, forming stable and evenly distributed Ag nanoparticle coated nanofibers. The immobilization of the NPs on the NC network prevents them from being released and hence minimizes the toxicity of the nanoparticles. The hybrid has been demonstrated to have high antibacterial activity against different bacteria and allow attachment as well as growth of epidermal cells with no cytotoxicity, resulting in a reduction in inflammation and fast wound healing. In the study carried out by Bie *et al.*,[224] the authors prepared a dual functional material based on nanocellulose, for efficient wound dressings, particularly useful for diabetic patients. The hybrid material consisting of CNFs with gentamicin (an antibacterial drug) was synthesized by electrospinning, and then these nanofibers were *in situ* modified by silver nanoparticles. The authors used gentamicin with the aim of healing the infection inflammation, while silver nanoparticles were used for their antibacterial activity. The thorough characterization of the cellulose/gentamicin/silver nanofibers has demonstrated excellent antibacterial properties as well as an appreciable drug release profile. Similarly, biofilms and hydrogels based on cellulose and zinc oxide nanostructures have been reported to have prominent applications as wound healing materials.[225,226] Hybrids of copper-containing bioactive glass and CNFs have been synthesized for angiogenic promotion in the chronic wound healing application.[227]

The antimicrobial abilities of these hybrids have not been limited to wound healing but have also been utilized for several other biomedical applications.[228] For example, the antimicrobial properties of cellulose–MOF hybrids have been utilized to develop self-disinfecting textile materials for antimicrobial applications and infection prevention.[229] Biodegradable biosorbents based on cellulose–MOF hybrids having excellent microbial inactivation capabilities have been reported by Duan *et al.*,[230] synthesized *via in situ* anchoring MOFs on TEMPO-oxidized corncobs.

Another subfield of biomedical applications, where the hybrids of nanocellulose are being extensively explored is guided bone regeneration, thanks to the three-dimensional structure of nanocellulose and the interconnected porosity, in addition to biocompatibility and degradability. Bone tissue is largely comprised of a matrix of different mineral forms of calcium phosphates and collagen, covering the osteoblasts, osteocytes, and lining cells. The treatment of bone diseases sometimes requires grafts/scaffolds, to repair the suffered area by inducing tissue regeneration. In this context, mineralization of the nanocellulose by calcium or phosphorous compounds provides unique ways to develop biocompatible materials. In a recent study, Jafari *et al.*[231] developed bimodal foams of phospho-calcified CNCs and poly-(ε-caprolactone) (PCL) and tested them for osteogenic differentiation of human mesenchymal stem cells. These scaffolds have been demonstrated to be a suitable option to mimic the architecture of the ECM. Moreover, it has been shown that the mechanical, hydrophilic, and biodegradability properties of the hybrids can be improved by simply increasing the concentration of the phospho-calcified CNCs. A. Cañas-Gutiérrez *et al.*[232] examined the effect of the surface groups (hydroxyl or carboxylate) of the bacterial cellulose on calcium phosphate precipitation for bone tissue engineering. For this purpose, the calcium phosphate mineralization process was carried out on the unmodified nanocellulose and TEMPO-oxidized cellulose scaffolds. It has been observed that the oxidation treatment in the TEMPO-oxidized cellulose scaffolds leads to the growth of the heterogeneously distributed microcrystals, while microcrystals are found to be homogeneously distributed in the unmodified nanocellulose scaffolds. The *in vitro* cell studies however show good cellular adhesion and high cell viability in both types of scaffolds. Hu *et al.*[233] presented the strategies to prepare bioabsorbable cellulose–calcium phosphate hybrids loaded with cellulosic enzymes for bone defect repair. The hybrid has been shown to be able to locally deliver calcium phosphate and to provide mechanical and nutrient support for cell growth. The hybrid acts as a temporary bone substituent and finally undergoes biodegradation by the enzyme. In another interesting study,[234] the multifunctional reinforced material of CNC–ZnO was prepared by *in situ* mineralization, using the one-step hydrothermal method. In the preparation method, CNC suspension was added into an aqueous solution of zinc chloride

and NaOH of suitable concentrations and stored at 80 °C for 24 h in an oven, resulting in the formation of nanohybrids. These ZnO–CNC hybrids as UV absorbers and antibacterial agents were then reinforced into bio-polyester *via* the electrospinning process. The nanohybrids have been found to enhance the thermal stability and crystallization ability of the biopolymer as well as having ultrahigh UV-shielding and antibacterial performances.

Not limited to the scaffolds for bone regeneration, recent extensive research has also shown NC hybrids to be one of the potential candidates that can be utilized in medical implants, *e.g.* cortical implants. The material used as an implant for soft-tissue replacement and reconstruction applications should have mechanical properties compatible with the tissue in terms of chemistry, mechanical, and pharmacological properties, along with biocompatibility, non-thrombogenicity, sterilizability, durability, and optimized degrees of calcification, as well as good and easy processability.[207] There is usually a compromise among these properties. For example, the cortical implant which can act as a neural interface is usually made up of metals that are much stiffer than brain tissues. The advantage of being stiffer is that these implants can be easily inserted into the soft brain tissue without buckling. However, the contact between the probe and the tissue significantly increases the risk of tissue damage and the death of the neurons, due to their incompatibility. It has been understood that such risks can be minimized if the mismatch between the mechanical properties of the implant and the soft body tissue can be minimized. Researchers are now more interested in implants made up of soft electrode materials and/or metal electrodes based on soft substrates such as cellulose.

In a study by Tang *et al.*, super-soft multichannel electrodes (Au–BC electrodes) have been developed by depositing gold layers *via* electron beam evaporation, on a thin substrate of BC for neural interfacing applications.[235] The developed Au–BC electrodes have been shown to possess several advantages over the normal metal or synthetic polymer-based electrodes, such as (i) better compliance, in terms of Young's modulus, which for cellulose is in between those of peripheral neural tissues and brain tissues, (ii) a significantly low bending stiffness around 10^{-4} times that of a polyimide-based Au electrode, (iii) high flexibility, robustness and possibility of multichannel design, with a single channel width as low as 5 microns, and (iv) high biocompatibility. *In vivo* recording of brain electric activity has demonstrated the great potential of these electrodes for neural interfacing applications.

Mineralized nanocellulose hybrids have also found application in the field of biosensing.[236–238] Recently, approaches have been explored to utilize cellulose hybrids for replacing the other polymeric materials used as supports for diagnostic devices. The use of cellulose facilitates the anchoring of the different biomolecules (adsorption of antibodies, enzymes, viruses, and polyelectrolytes) and configures the basis for biomedical devices intended for cellular growth screening as well as for studying cell-signaling mechanisms. For example, BC has been shown to have the ability to anchor high amounts of IgG for the detection of dengue viruses in plasma samples.[239] On the other hand, the inorganic components of the hybrids provide additional advantages for generating and collecting the detectable signals as well as for improving the sensitivity and selectivity of diagnostic devices.

In a study by Li *et al.*,[240] hybrid nanofibers of palladium nanoparticles and BC were synthesized by employing an *in situ* chemical reduction method. These nanofibers were then mixed with laccase and Nafion and the mixture was employed to modify the electrode surface to construct a novel biosensing platform. While evaluating the electrochemical performance of the modified electrodes, acceleration of the electron transfer and weakening of the interface resistance have been observed and attributed to the good electron conductivity and catalytic abilities of palladium nanoparticles. The developed biosensor has been shown to exhibit excellent bioelectrocatalysis towards dopamine, present in human urine, with high sensitivity, low detection limit, and wide linear range, along with good repeatability, reproducibility, selectivity, and stability.

An aptamer-based cellulose acetate–MoS_2 nanopetal hybrid biosensor has also been fabricated for the diagnosis of acute myocardial infarction.[241] In this work, petal-like MoS_2 nanoflowers acted as an active material for AMI biomarker determination. The three-dimensional microstructure generated by 1D cellulose nanofibers and 2D MoS_2 flower-like nanosheets provided many pores for the immobilization and interaction processes. The sensors prepared using these hybrids have attained a very low limit of detection, high sensitivity, and good reproducibility, and can detect multiple biomolecules on a single sensing platform.

There is also a lot of recent interest in cellulose paper-based hybrid biosensors for medical diagnostics, owing to their low cost and high sensitivity and performance.[242–244] The microporous structure of these paper-based devices not only offers sufficient space for storing immobilized analytical reagents but also drives capillary force to guide liquid samples towards a dedicated reaction zone for almost instantaneous detection of the analytes. The mineralization of the cellulose in these paper-based sensors improves several key parameters, such as selectivity, efficiency, sensitivity, dynamic range, the limit of detection, *etc.* The silver nanoparticle embedded cellulose nanopaper based sensors have been shown to be capable of the detection of the cyanide ion (CN^-) and 2-mercaptobenzothiazole (MBT). In this work, hydroxyl groups of CNFs were utilized to reduce the adsorbed silver ions on nanopaper. Similarly, a novel, disposable, inexpensive paper-based assay has been realized for rapid, enzyme-free, and colorimetric determination of the glucose level by *in situ* synthesis of gold nanoparticles in cellulose paper.[245] In short, mineralized nanocellulose provides synergistic advantages that cannot be possessed by individual components or synthetic polymer-based hybrids and hence has enormous potential in the field of biomedicine.

6.4. Hybrid materials for energy and electronics

There is emerging interest in natural polymers for their applications in the field of energy/electronics, particularly for developing novel devices with unique features, *e.g.*

stretchability, self-healing, and flexibility.[7,246–252] Nanocellulose with its excellent physical properties (high transparency, low coefficient of thermal expansion, and flexibility with good mechanical strength), dielectric and piezoelectric properties, and ability to be functionalized with a variety of molecules is a suitable candidate for the development of electronic devices.[7,246–259] The incorporation of a biocompatible and biodegradable polymer like nanocellulose not only provides flexibility and stretchability to these electronic devices but also eases the environmental load that is increasing day by day due to the tonnes of non-degradable electronic waste.

The area of printed electronics utilizes electronically functional inks for large-area fabrication by employing traditional printing methods (*e.g.*, screen printing, inkjet printing, and flexography). This can be taken a step forward by designing the electronics on a flexible and biodegradable substrate such as plastic or paper.[7,246–252,258,259] In this regard, the utilization of NC opens pathways not limited to a paper substrate but it also plays an important role in hybrid materials, providing mechanical strength, favorable 3D-microstructures, and the above listed additional advantages, which are not possible with other flexible substrates like plastic. Moreover, NC, in particular CNFs, is emerging as a substitute for classical electronic packaging materials (*e.g.*, resins, glass, plastics, *etc.*). In addition, CNFs make large-scale roll-to-roll production relatively easier, due to the compatible mechanical properties.[249] There can be several other plastic/organic substrates that can be utilized for the fabrication of flexible devices but face the limitation of the performance against thermal stress. The difference in the thermal coefficients of the plastic substrate and the other elements of the instrument leads to significant thermal stress not only in the fabrication process but also during long-term operation, resulting in the malfunctioning of the device, and most of the time, failure. The use of cellulose-based photopatternable, flexible and stretchable substrates has been shown to overcome such limitations by reducing the thermal expansion coefficients. Cellulosic materials possess a sufficiently low coefficient of thermal expansion (as low as 0.1 ppm K^{-1}),[251] as required for the components of electronic devices that are known to produce heat. Other polymers such as polyethylene terephthalate and polyethylene naphthalate can also provide an alternative for flexibility but these are known to have a large carbon footprint, as well as generate harmful waste, unlike cellulose.[257]

The utilization of NC in electronics many times requires its hybridization with some conductive material, for instance, metal or metal oxide nanoparticles,[260–264] semiconducting nanostructures,[265,266] carbon materials (not covered in this article), *etc.* Functional materials produced *via* mineralization of NC have shown enormous potential for intelligent, portable, and flexible electronics, covering a wide range of instruments, *e.g.*, smart sensors including biomimetic electronic skins or detection devices, optoelectronics and energy storage devices, ionic conductors, supercapacitor batteries, and triboelectric nanogenerators as well as electrolytes and electrode materials required for the design of conventional electronic equipment such as transistors, *etc.*[252,267] In a recent report, flexible electrodes of very low sheet resistance and high transparency have been demonstrated by combining cellulose nanopaper with silver nanowires. It is important to mention here that high transparency with low haze nanopaper was achieved by hybridization of CNFs and CNCs.[102] Similarly, a freestanding electrochromic paper-like electrode has been designed using a cellulose composite comprising poly(3,4-ethylene dioxythiophene) polystyrene sulfonate (PEDOT:PSS) as the electrochromic material hybridized with TiO_2 nanoparticles as the reflecting material.[268] A combination of colloidal ZnO nanorods and laminated cellulose ionogels has been utilized to fabricate the electrolyte-gated, flexible field-effect transistors on paper.[269] Moreover, in very recent and interesting work, highly conductive ferroelectric cellulose hybrid paper was synthesized consisting of BC with silver nanowires and $BaTiO_3$ nanoparticles. These hybrid papers have been successfully used to fabricate a large-area triboelectric nanogenerator with excellent electrical output performance. The percolated network of the silver nanowires in the cellulose fibers results in high electrical conductivity and enables the paper to serve as a positive triboelectric layer as well as a bottom electrode, with no requirement for placing an additional electrode. Moreover, the addition of the $BaTiO_3$ nanoparticles provides ferroelectric character to the paper which in turn supports the easy charge transfer between the paper and triboelectric layer, resulting in increased output performance.[270]

The potential of cellulose-based materials for chemical and biosensor applications has also been emerging as a field of recent interest.[246] A transparent and flexible fingerprint sensor array has been recently developed by combining silver nanowires/fibers with CNFs. The arrays have been designed with the ability for multiplexed detection of tactile pressure and skin temperature for use in mobile smart devices.[271] A transparent photoluminescent hybrid film composed of Eu-MOF and TOCNF has been reported for specifically detecting copper ions. The nano Eu-MOF was synthesized *in situ* on the surface of TOCNF in hydroalcoholic medium and the resulting film has been shown to have high selectivity toward copper ions.[272]

One of the most interesting developments regarding cellulose and flexible electronics is the generation of wood-based electronic devices. In a recent report, a fully wood-based flexible electronic circuit has been printed on a strong, flexible, and transparent wood film, with a lignin-derived carbon nanofiber conductive ink.[273] A transparent paper touchscreen composed of nanocellulose hybrid paper as a flexible electrode, having an excellent anti-glare effect, has been developed.[102,274] A new type of wood-based material having the ability to bend and roll without loss of electrical function has been prepared by reinforcement of nanosilicate in nanocellulose with potential applications in flexible electronics.[257] Electrically conducting wood (regenerated cellulose) based yarns have been fabricated employing a roll-to-roll coating process with the ink of a biocompatible polymer. The electrical conductivity of the yarn has further been enhanced by the incorporation of Ag nanowires.[275] For flexible electronics such as foldable smartphones, curved displays, and smartwatches to become the marvel of this modern age, the aforesaid design concepts for sustainable

development of next-generation flexible electronics is essentially required.

In addition to the novel applications of cellulose in the field of electronics as shown heretofore, there is great interest in finding and establishing alternative, efficient and renewable ways to develop ECS (energy conversion and storage) technologies. Commonly, ECS technologies are known for their environment friendliness and renewability involving water splitting and redox processes *via* photocatalysis (light-harvesting, electron–hole separation) and electrocatalysis (fuel cells, metal–air batteries (MABs)).[276] Besides, electrochemical energy storage is emerging as an eco-friendly technology to develop supercapacitors and metal-ion batteries. Although use of the aforesaid techniques has already begun in the application sector of automobiles, integrated electronics, and smart homes, they still have several challenges due to high catalyst costs and limited shelf life. To name a few of these challenges, the following are of current interest: (i) due to the limited area for light absorption, conventional photocatalysts often exhibit inefficient light-harvesting, resulting in prolonging the transportation of carriers between holes and electrons; (ii) besides, choosing a complex route to obtain photocatalysts leads to lack of porosity and stability (emergence of metal dendrites),[276] (iii) electrocatalysts, on the other hand, require additional energy due to their slow reaction dynamics (sluggish redox recharging in MABs), shuttle effect (lithium–sulfur batteries) and low electrical conductivity.[277] To overcome these shortcomings and exclusively in the area of sustainable growth, several strategies have been proposed to obtain multifunctionality *via* engineered nanostructures, enhanced porosity (rapid kinetics, better rechargeability), or using a large number of active sites to increase absorption.[276–279] Due to adjustable metal nodes and tunable organic linkers, MOFs have made staggering progress in developing multifunctional materials to facilitate efficient ECS technologies.[280–283] Structural control (coordination bonding) *via* MOFs offers superior porosity; hence the higher number of active sites (achieved by adjusting the physical aspects of pores) allows spatial ordering and efficient host–guest interactions.[276–283] Recent reports on introducing different metal centers such as Co(II), Ni(II), and Cu(II) have shown improved charge delocalization using π-conjugated ligands (organic and metal-based).[277–280] Stacking the conjugated nanostructures greatly enhances charge interactions and redox reactive sites, resulting in efficient thermogravimetric capacitance.[284]

Nanocellulose combined with other nanoparticles can possess functionality also for energy applications. Zhou *et al.*[284] proposed a strategy to prepare conductive metal–organic framework (c-HHTP, c-HITP) nanopapers *via in situ* growing the porous coordination polymers on CNFs (CNF@c-MOF) and subsequently forming a hybrid nanopaper (Fig. 8(a)), demonstrating hierarchical micro/mesoporosity, high conductance (100 S cm^{-1}), and high mechanical strength. Building pristine c-MOFs with controlled morphology and architectural flexibility (nanofibers or nanosheets) is greatly challenged by their crystalline and inert nature.[285,286] This study, however, demonstrates a sustainable approach to engineer flexible nanopapers with continuous nucleation of c-MOF nanolayers on carboxylated CNFs *via* interfacial synthesis. In a similar approach (see Fig. 8(a) and (b) for comparison), *Cladophora* algae-derived CNFs were carboxylated (*via* TEMPO-mediated oxidation), followed by ion exchange with Ni^{2+} ions. Subsequently, the addition of $6H_2O$ and 2,3,6,7,10,11-hexahydroxytriphenylene (HHTP) or HITP resulted in Ni-HHTP and Ni-HITP c-MOFs. Vacuum filtration of a homogenized suspension of CNF@c-MOFs over a 0.1 μm membrane formed the flexible nanopapers. X-ray diffraction (XRD) revealed reduced *d*-spacing indicating c-MOFs grown on CNFs, thereby indicating efficient π–π stacking interaction ensuring high electrical conductivity.[287–289] Moreover, transmission electron microscopy (TEM) and X-ray photoelectron spectroscopy (XPS) substantiated the interfacial growth and uniform integration of a Ni-HITP on the CNF surface (CNF@Ni-HITP). The tensile strength of the materials was 350 MPa and Young's modulus was 10 GPa. Fig. 8(e) and (f) highlight the flexibility illustrated by the origami folded flower and its resistance to bending. In addition, porosity features span from micropores (~1.5 nm) to mesopores (~15–50 nm). The conductivity of CNF@c-MOFs is 1–2 orders of magnitude larger when compared to the c-MOF pellets, possibly caused by the continuous nanolayer growth while shortening the interparticle cavities. To use this as an electrode, the nanopapers were immersed as an asymmetric three-electrode set-up in a 3 M KCl aqueous electrolyte bath without any binders or conductive additives (Fig. 8(c)). In contrast to the reference electrode, Ag/AgCl and platinum wire showed higher capacitance, with 70% recovery on 100 times increase in current density. Besides, conductivity and flexibility can be easily tuned by varying the nanopaper thickness by controlling the c-MOF content. On this premise, such a customizable nanostructure of CNF@c-MOFs efficiently facilitating charge transfer, fast electrolyte ion exchange, mechanical stability, and high flexibility makes it a viable candidate for a supercapacitor, sparking excellence in electrochemical performance. The supercapacitor (1.5 cm × 2.0 cm × 0.005 cm) is a sandwich assembly of two identical CNF@Ni-HITP nanopaper electrodes separated by a filter paper, while graphite foils were used as current collectors in an electrolytic gel of poly(vinyl alcohol) (PVA) dissolved in aqueous KCl. Cyclic voltammetry (CV) and galvanostatic charge/discharge (GCD) were extensively used to evaluate the electrical performance of the CNF@Ni-HITP supercapacitor, revealing comparable if not superior capacitance, energy storage, and power consumption, in comparison to the state-of-the-art MOF-based supercapacitors. Moreover, in a recent study, the development of a hybrid film consisting of a conductive MOF layered on CNFs having the ability for efficient solar power generation has been demonstrated. It has been shown that a large thermal gradient on the surface under light illumination resulting from the strong light absorption and low thermal conductivity of the film induces fast water evaporation in an aqueous electrolyte. This leads to selective ion transport through the charged nanochannels, generating ionic thermoelectric and streaming potentials. Finally, the device has been shown to produce a sustained voltage output of about 1.1 V, along with a power density of up to 15 W m^{-2} under one sun.[290]

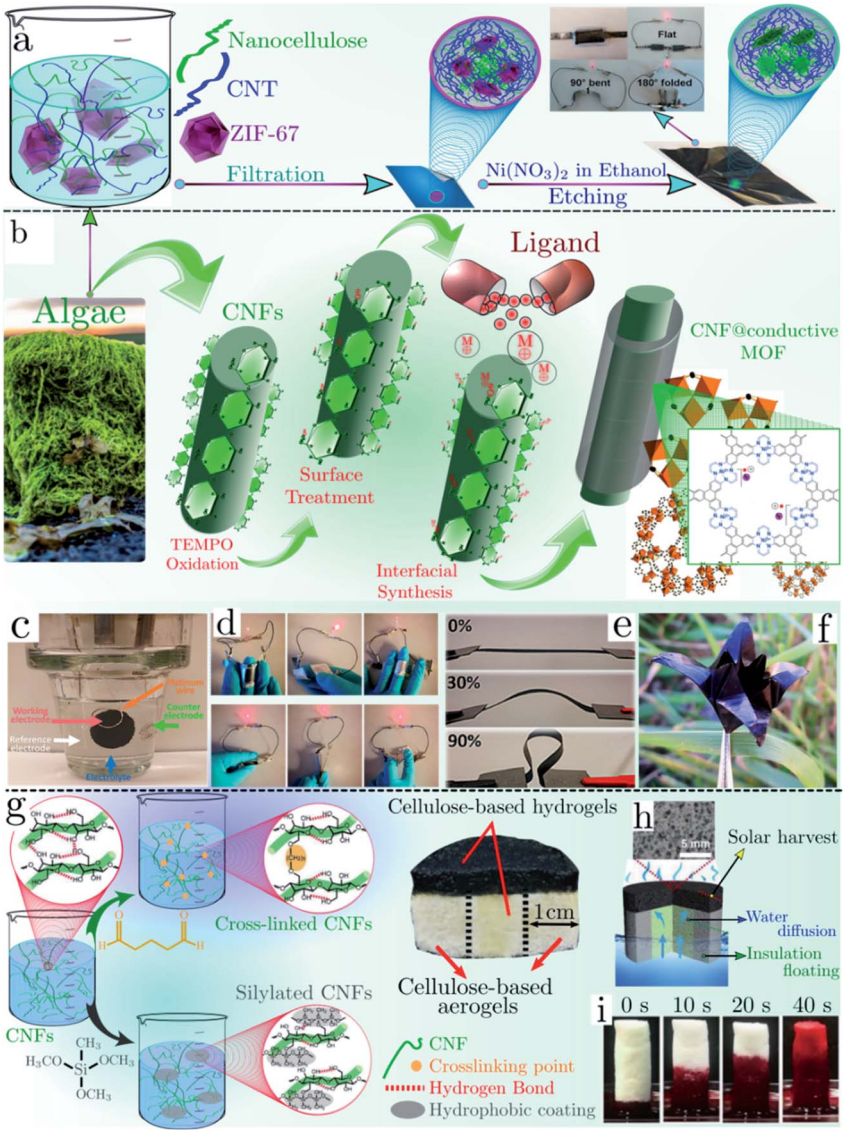

Fig. 8 An overview to promote mineralized cellulose in ECS technologies. (a) and (b) demonstrate two separate routes to obtain (a) nanosheets (LDH-CC-CNT; *Cladophora* cellulose)[291] and (b) hybrid nanofibers (CNFs@c-MOF)[311] while sharing a common source to obtain nanocellulose, "algae". Images shown in (a) and (d) capture the red LEDs powered by the developed nanosheets in (a) and hybrid CNFs@c-MOF in (b), respectively, uninterrupted by the applied deformations. (c) Common three-electrode-based protocol to test ECS performance (*e.g.*, cyclic voltammetry, galvanostatic charge/discharge, gravimetric capacitance, and electrochemical impedance), as shown for CNFs@c-MOF electrodes immersed in 3 M KCl aqueous solution. (e) Flexible features as corroborated by the normalized resistance of CNFs@-Ni-HITP to bending. (f) Image illustrating an origami lily flower complementing the versatility of the developed nanopaper by CNF@c-MOF. (g) Schematic approaches to obtain chemically modified multifunctional gels to fabricate the all-cellulose-based 3D hybrid steam generator.[303] (h) Digitized sketch to illustrate interfacial steam generators and their functions. (i) Effective water diffusion process in cross-linked CNFs.

Similarly, a study by Xu *et al.* has highlighted the development of hierarchical porous and conductive nanosheets based on a Co-based MOF and CNFs to be utilized as flexible and foldable electrodes for energy storage devices.[291]

Although established, rechargeable batteries are still rapidly growing, to satisfy this supply–demand chain, especially in an environmentally friendly manner to alleviate the disposal of used batteries which has become a global concern.[292–298] Besides, upon incineration, batteries lead to the production of CO_2 and the release of harmful substances (often non-biodegradable).[293–298] Recently, technologies for recycling batteries have been rapidly emerging and promoting a cleaner outlook; however cost-effective strategies and residue-less recycling still need to be achieved.[294–297] Several reports[294–296,299–302] on using biodegradable materials are beginning to acknowledge the aforesaid issues but they are developed to replace an individual or some components of a battery, thus preventing the elimination of non-biocompatible materials. The readers who wish to go deeper in detail are encouraged to study the references heretofore given.

Apart from the use of nanocellulose as a filter for water purification (discussed in a previous subsection), the

mineralized cellulose-based triboelectric nanogenerator has also attracted attention for achieving low-cost water purification, seawater desalination, and distillation. In this regard, the recent work[303] of Li *et. al.* proposed a concept of bacterial cellulose (BC) based self-powered 3D steam generator with well-defined hybrid structures integrated with a TENG (triboelectric nanogenerator) in solar-driven interfacial evaporation applications. The conventional designs for solar stills where a hydrophilic absorber is directly floated on the water surface facilitating environmental energy input and vaporization enthalpy recycling have been heavily criticized for their low photothermal efficiencies as the counterproposals of employing an indirect contact approach introducing a sponge-like substrate is favoured.[303] However, this indirect contact approach can be expensive due to limited material selection, and the high risk of releasing microplastics into the environment also makes it challenging for mass production. Thus, this study puts forth a concept design by fine-tuning the CNFs to construct a dual-reinforced network of hydrophilic CNF aerogels *via* crosslinking by glutaraldehyde and freeze-drying, which was then fabricated to float over the hydrophobic CNF aerogels, obtained by silylation in the presence of methyltrimethoxysilane (MTMS) in acidic medium, ensuring covalent and hydrogen bonding and satisfactory near-optimal resolution in the contact angle, wettability, water storage, transport, and mechanical strength (Fig. 8(g)). The prime benefit of dual crosslinking in contrast to the CNF aerogel with hydrogen bonding is high resistance to applied deformation in both wet and dry conditions. As shown in Fig. 8(h), the 3D hybrid pillared steam generator was assembled using three key all-cellulose materials, (i) CNFs-g50 as a water path, (ii) CNFs-g50/CB (nanocarbon black, CB) as a solar absorber, and (iii) CNF-Si60 as a floater. In contrast to previous 3D monolithic steam generators,[303–306] where maintaining low density in water was reported to be the common issue, this design achieves this inevitably by keeping the mass and buoyancy of each element in balance, preventing overall heat losses.[303] The most important characteristic of this "indirect contact" strategy making the 3D monolithic steam generator reviewed here far more superior than its predecessors[303–306] is the isolation of the solar absorber over water, allowing light-to-heat conversion localized only on its surface resulting in high photothermal efficiency, fast evaporation, effective thermal insulation, and high solar absorptance. Furthermore, the 3D hybrid steam generator was tested under harsh water conditions as one might face in aquatic environments and/or industrial sites. On a pH scale of 1–13, spanning from acid rain and industrial wastewater to cleaning reagents, the water evaporation rate was found to be unaffected under sunlight, offering structural and functional durability in strongly acidic or alkaline environments, with a high elimination rate of rejecting salts in saline water. This additional salt-rejecting feature is another complement to the indirect contact design concept presented in this study, where the hydrophilic networks of CNFs-g50 utilize their equilibrated state to redissolve and diffuse back the salt sediments into the brine, and the hydrophobic CNFs-Si60 inhibits adhesion of salt crystals. In order to be employed in open water systems and ensure efficient water wave detection, this 3D hybrid steam generator was integrated with a self-powered TENG, which has been previously demonstrated to be efficient in detecting oscillatory motions and also providing strong support for blue energy harvesting in oceans.[303,307–309] The generator has been found to be steady and performed uninterruptedly in detecting ocean waves when tested against wind-generated waves and atmospheric pressure gradients. With such a high mechanical robustness and multifunctionality, this monolithic design strategy for a 3D hybrid steam generator with a self-powered TENG would indeed serve as a model for mass production in the future to be deployed not only for water purification and recovery, and desalination but also in maintaining the sustainability of marine life and weather forecasting.

7. Conclusions

The overall aim of the present review is to summarize the current research status as well as interests in introducing unique and extraordinary capabilities in nanocellulose *via* its mineralization, for enabling its utilization in a wide range of advanced applications. Cellulose as the most abundant, biodegradable and renewable biopolymer offers its candidature as a substitute for synthetic polymers and sustainable material with minimum environmental load, for a variety of applications. In "nano-configuration", nanocellulose based materials constitute a new class of bio-based "building blocks" that are inspiring advances for the next generation of high-performance sustainable materials.

However, certain inherent limitations of nanocellulose (*e.g.*, low conductivity, high susceptibility to chemical changes, vulnerability to microbial decay, low compatibility with hydrophobic solvents/materials, *etc.*) restrict its performance. These limitations can be overcome by mineralizing the nanocellulose with suitable inorganic components (*e.g.* metals, metal oxides, silicates, metal–organic frameworks, *etc.*), which has proven to be an attractive path towards the optimal expression of properties brought together by multiple components in one single material from 2D/3D materials. This strategy can also be used to introduce further functionalities which are normally not present in NC-based materials, such as gas separation capabilities and photocatalytic activity. Moreover, some mineralization strategies can also be performed under ambient conditions using green chemistry methods. They can also be fully scalable with existing infrastructure.

Nanocellulose is an excellent building block to design functional nanomaterials by mineralization, owing to (among many other properties) its excellent mechanical properties, ease of processability into porous 2/3D structures, and highly reactive surface with high surface area (leading to the high density of *in situ* grown subcomponents, and thus high functionality). The physical properties of hybrid materials essentially depend on the chemical composition of the phases (nanocellulose + metal–organic frameworks/metal oxide nanoparticles, *etc.*), the types of interactions within the components that form the hybrid (chemical or physical crosslinking), the chemical pathways that are used to design a given hybrid material, and the

processing method/conditions used to form the final 2D (films, membranes) or 3D (foams, aerogels, scaffolds, *etc.*) material.

Based on the design parameters and mineralized components, unique features (*e.g.*, self-healing, improved structural integrity, hygroscopicity, magnetic character, photocatalytic activity, antimicrobial properties, conductivity, *etc.*) can be invoked in the hybrid materials. The review article discusses several examples from recent reports where the mineralization of nanocellulose has been employed for its efficient utilization in the fields of current interest for mankind, such as gas (in particular CO_2) absorption, water purification, biomedical applications, stretchable and flexible electronics, energy storage devices, *etc.* There is however still ample scope for further research activities focused on developing new and innovative synthesis methods, optimizing process parameters, and using the wide range of available inorganic precursors, to obtain materials with improved properties and multiple functionalities.

Conflicts of interest

There are no conflicts to declare.

References

1 J. P. F. Lagerwall, C. Schütz, M. Salajkova, J. Noh, J. Hyun Park, G. Scalia and L. Bergström, *NPG Asia Mater.*, 2014, **6**, e80.
2 P. Kaur, N. Sharma, M. Munagala, R. Rajkhowa, B. Aallardyce, Y. Shastri and R. Agrawal, *Front. Nanotechnol.*, 2021, 82.
3 K. Heise, E. Kontturi, Y. Allahverdiyeva, T. Tammelin, M. B. Linder, Nonappa and O. Ikkala, *Adv. Mater.*, 2021, **33**, 2004349.
4 K. Dhali, M. Ghasemlou, F. Daver, P. Cass and B. Adhikari, *Sci. Total Environ.*, 2021, **775**, 145871.
5 R. J. Moon, G. T. Schueneman and J. Simonsen, *JOM*, 2016, 2383–2394.
6 X. Du, Z. Zhang, W. Liu and Y. Deng, *Nano Energy*, 2017, **35**, 299–320.
7 S. Agate, M. Joyce, L. Lucian and L. Pal, *Carbohydr. Polym.*, 2018, **198**, 249–260.
8 F. Hoeng, J. Bras, E. Gicquel, G. Krosnicki and A. Denneulin, *RSC Adv.*, 2017, **7**, 15372–15381.
9 Q. Chen, R. P. Garcia, J. Munoz, U. Pérez De Larraya, N. Garmendia, Q. Yao and A. R. Boccaccini, *ACS Appl. Mater. Interfaces*, 2015, **7**, 24715–24725.
10 M. Oprea and D. M. Panaitescu, *Molecules*, 2020, **25**, 4045.
11 A. Rahman, V. S. R. R. Pullabhotla, L. Daniel and V. Uahengo, *Cellul. Nanocrystal/Nanoparticles Hybrid Nanocomposites*, 2021, 141–164.
12 H. Zhu, X. Yang, E. D. Cranston, S. Zhu, H. Zhu, X. Yang, E. D. Cranston and S. Zhu, *Adv. Mater.*, 2016, **28**, 7652–7657.
13 L. Johnson, W. Thielemans and D. A. Walsh, *J. Mater. Chem.*, 2010, **20**, 1737–1743.
14 M. Kaushik and A. Moores, *Green Chem.*, 2016, **18**, 622–637.
15 Y. Zhan, Y. Meng, W. Li, Z. Chen, N. Yan, Y. Li and M. Teng, *Ind. Crops Prod.*, 2018, **122**, 422–429.
16 Y. Shchipunov and I. Postnova, *Adv. Funct. Mater.*, 2018, **1705042**, 1–28.
17 P. G. Gan, S. T. Sam, M. F. bin Abdullah and M. F. Omar, *J. Appl. Polym. Sci.*, 2020, **137**, 48544.
18 D. Trache, A. F. Tarchoun, M. Derradji, T. S. Hamidon, N. Masruchin, N. Brosse and M. H. Hussin, *Front. Chem.*, 2020, 392.
19 H. Kargarzadeh, J. Huang, N. Lin, I. Ahmad, M. Mariano, A. Dufresne, S. Thomas and A. Gałęski, *Prog. Polym. Sci.*, 2018, 197–227.
20 D. Roy, M. Semsarilar, J. T. Guthrie and S. Perrier, *Chem. Soc. Rev.*, 2009, **38**, 2046–2064.
21 Y. Habibi, *Chem. Soc. Rev.*, 2014, **43**, 1519–1542.
22 A. Chakrabarty and Y. Teramoto, *Polymers*, 2018, 517.
23 K. J. Nagarajan, N. R. Ramanujam, M. R. Sanjay, S. Siengchin, B. Surya Rajan, K. Sathick Basha, P. Madhu and G. R. Raghav, *Polym. Compos.*, 2021, **42**, 1588–1630.
24 A. Isogai and L. Bergström, *Curr. Opin. Green Sustain. Chem.*, 2018, **12**, 15–21.
25 H. P. S. Abdul Khalil, Y. Davoudpour, M. N. Islam, A. Mustapha, K. Sudesh, R. Dungani and M. Jawaid, *Carbohydr. Polym.*, 2014, **99**, 649–665.
26 S. Eyley and W. Thielemans, *Nanoscale*, 2014, **6**, 7764–7779.
27 S. Eyley, C. Schütz and W. Thielemans, in *Cellulose Science and Technology*, John Wiley & Sons, Inc., Hoboken, NJ, USA, 2018, pp. 223–252.
28 M. S. Reid, M. Villalobos and E. D. Cranston, *Langmuir*, 2017, 1583–1598.
29 S. Gorgieva and J. Trček, *Nanomaterials*, 2019, **9**, 1352.
30 U. G. K. Wegst, H. Bai, E. Saiz, A. P. Tomsia and R. O. Ritchie, *Nat. Mater.*, 2015, **14**, 23–36.
31 G. M. Luz and J. F. Mano, *Compos. Sci. Technol.*, 2010, **70**, 1777–1788.
32 N. S. Ha and G. Lu, *Compos. Part B Eng.*, 2020, **181**, 107496.
33 Y. Xu, F. Nudelman, E. D. Eren, M. J. M. Wirix, B. Cantaert, W. H. Nijhuis, D. Hermida-Merino, G. Portale, P. H. H. Bomans, C. Ottmann, H. Friedrich, W. Bras, A. Akiva, J. P. R. O. Orgel, F. C. Meldrum and N. Sommerdijk, *Nat. Commun.*, 2020, **11**, 5068.
34 G. Huajian, J. Baohua, J. I. L. Ingomar, A. Eduard and F. Peter, *Proc. Natl. Acad. Sci.*, 2003, **100**, 5597–5600.
35 H. Gao, *Int. J. Fract.*, 2006, **138**, 101.
36 A. Ghazlan, T. Ngo, P. Tan, Y. M. Xie, P. Tran and M. Donough, *Compos. Part B Eng.*, 2021, **205**, 108513.
37 A. Ilyas Rushdana, M. Sapuan Salit, M. Lamin Sanyang and M. Ridzwan Ishak, *Curr. Anal. Chem.*, 2018, **14**, 203–225.
38 W. E. Hennink and C. F. van Nostrum, *Adv. Drug Deliv. Rev.*, 2012, **54**, 13–36.
39 J. A. Hunt, R. Chen, T. van Veen and N. Bryan, *J. Mater. Chem. B*, 2014, 5319–5338.
40 H. N. Abdelhamid and A. P. Mathew, *Coord. Chem. Rev.*, 2022, **451**, 214263.
41 A. A. Oun, S. Shankar and J. W. Rhim, *Crit. Rev. Food Sci. Nutr.*, 2019, **60**, 435–460.

42 S. Pandey and S. B. Mishra, *J. Sol-Gel Sci. Technol.*, 2011, **59**, 73–94.
43 T. Adschiri and K. Byrappa, *Chem. Lett.*, 2009, 247–280.
44 A. P. Carapeto, A. M. Ferraria and A. M. Botelho do Rego, *Polym. Test.*, 2017, **58**, 236–240.
45 L. Valencia, E. M. Nomena, S. Monti, W. Arbelaez, A. Mathew, S. Kumar and K. P. Velikov, *Nanoscale*, 2020, 15652–15662.
46 C. Salas, T. Nypelö, C. Rodriguez-Abreu, C. Carrillo and O. J. Rojas, *Curr. Opin. Colloid Interface Sci.*, 2014, **19**, 383–396.
47 C. Honorato-Rios and J. P. F. Lagerwall, *Commun. Mater.*, 2020, **1**, 69.
48 D. Shen, J. Liu, L. Gan, N. Huang and M. Long, *RSC Adv.*, 2017, **7**, 19237–19242.
49 L. Valencia, S. Kumar, E. M. Nomena, G. Salazar-Alvarez and A. P. Mathew, *ACS Appl. Nano Mater.*, 2020, **3**, 7172–7181.
50 Y. Qi, Z. Cheng, Z. Ye, H. Zhu and C. Aparicio, *ACS Appl. Mater. Interfaces*, 2019, **11**, 27598–27604.
51 Z. Cheng, Z. Ye, A. Natan, Y. Ma, H. Li, Y. Chen, L. Wan, C. Aparicio and H. Zhu, *ACS Appl. Mater. Interfaces*, 2019, **11**, 42486–42495.
52 M. Wu, P. Wu, L. Xiao, Y. Zhao, F. Yan, X. Liu, Y. Xie, C. Zhang, Y. Chen and L. Cai, *Int. J. Biol. Macromol.*, 2020, **162**, 1627–1641.
53 P. Mohammadi, J.-A. Gandier, Nonappa, W. Wagermaier, A. Miserez and M. Penttilä, *Adv. Mater.*, 2021, **33**, 2102658.
54 D. Y. Zaki, E. M. Safwat, S. M. Nagi, H. N. Salem, T. M. Hamdy, L. M. Moharam, M. L. Hassan and E. M. A. Hamzawy, *Carbohydr. Polym. Technol. Appl.*, 2021, **2**, 100035.
55 C. Zhou, Z. Chen, H. Yang, K. Hou, X. Zeng, Y. Zheng and J. Cheng, *ACS Appl. Mater. Interfaces*, 2017, **9**, 9184–9194.
56 Z. Dai, J. Guo, T. Su, J. Wang, Z. Gao and Y.-Y. Song, *Green Chem.*, 2021, **23**, 8685–8693.
57 Q. Zhang, L. Zhang, W. Wu and H. Xiao, *Carbohydr. Polym.*, 2020, **229**, 115454.
58 M. Kaushik, K. Basu, C. Benoit, C. M. Cirtiu, H. Vali and A. Moores, *J. Am. Chem. Soc.*, 2015, **137**, 6124–6127.
59 M. Goswami and A. M. Das, *Carbohydr. Polym.*, 2018, **195**, 189–198.
60 C. N. Wu, S. C. Fuh, S. P. Lin, Y. Y. Lin, H. Y. Chen, J. M. Liu and K. C. Cheng, *Biomacromolecules*, 2018, **19**, 544–554.
61 M. Schlesinger, M. Giese, L. K. Blusch, W. Y. Hamad and M. J. MacLachlan, *Chem. Commun.*, 2015, **51**, 530–533.
62 R. Singla, S. Soni, P. M. Kulurkar, A. Kumari, S. Mahesh, V. Patial, Y. S. Padwad and S. K. Yadav, *Carbohydr. Polym.*, 2017, **155**, 152–162.
63 B. Heli, E. Morales-Narváez, H. Golmohammadi, A. Ajji and A. Merkoçi, *Nanoscale*, 2016, 7984–7991.
64 L. Huang, C. Wu, L. Xie, X. Yuan, X. Wei, Q. Huang, Y. Chen and Y. Lu, *Nanomaterials*, 2019, **9**, 355.
65 Y. Li, L. Xu, B. Xu, Z. Mao, H. Xu, Y. Zhong, L. Zhang, B. Wang and X. Sui, *ACS Appl. Mater. Interfaces*, 2017, **9**, 17155–17162.
66 A. Farooq, M. K. Patoary, M. Zhang, H. Mussana, M. Li, M. A. Naeem, M. Mushtaq, A. Farooq and L. Liu, *Int. J. Biol. Macromol.*, 2020, **154**, 1050–1073.
67 J. Li, R. Cha, K. Mou, X. Zhao, K. Long, H. Luo, F. Zhou and X. Jiang, *Adv. Healthc. Mater.*, 2018, 1800334.
68 Y. Cui, B. Li, H. He, W. Zhou, B. Chen and G. Qian, *Acc. Chem. Res.*, 2016, 483–493.
69 H.-C. J. Zhou and S. Kitagawa, *Chem. Soc. Rev.*, 2014, **43**, 5415–5418.
70 C. A. Trickett, A. Helal, B. A. Al-Maythalony, Z. H. Yamani, K. E. Cordova and O. M. Yaghi, *Nat. Rev. Mater.*, 2017, **2**, 17045.
71 L. Jiao, J. Y. R. Seow, W. S. Skinner, Z. U. Wang and H. L. Jiang, *Mater. Today*, 2019, 43–68.
72 R. B. Lin, S. Xiang, H. Xing, W. Zhou and B. Chen, *Coord. Chem. Rev.*, 2019, 87–103.
73 Z. Bao, G. Chang, H. Xing, R. Krishna, Q. Ren and B. Chen, *Energy Environ. Sci.*, 2016, 3612–3641.
74 K. Adil, Y. Belmabkhout, R. S. Pillai, A. Cadiau, P. M. Bhatt, A. H. Assen, G. Maurin and M. Eddaoudi, *Chem. Soc. Rev.*, 2017, **46**, 3402–3430.
75 J. D. Xiao, Q. Shang, Y. Xiong, Q. Zhang, Y. Luo, S. H. Yu and H. L. Jiang, *Angew. Chem., Int. Ed.*, 2016, **55**, 9389–9393.
76 P. Q. Liao, J. Q. Shen and J. P. Zhang, *Coord. Chem. Rev.*, 2018, 2838–2843.
77 J. Qiu, X. Zhang, Y. Feng, X. Zhang, H. Wang and J. Yao, *Appl. Catal. B Environ.*, 2018, 231–270.
78 H. Wang, Q. L. Zhu, R. Zou and Q. Xu, *Chem*, 2017, 52–80.
79 H. Zheng, Y. Zhang, L. Liu, W. Wan, P. Guo, A. M. Nyström and X. Zou, *J. Am. Chem. Soc.*, 2016, **138**, 962–968.
80 V. Stavila, A. A. Talin and M. D. Allendorf, *Chem. Soc. Rev.*, 2014, **43**, 5994–6010.
81 J. Ren, X. Dyosiba, N. M. Musyoka, H. W. Langmi, M. Mathe and S. Liao, *Coord. Chem. Rev.*, 2017, 187–219.
82 P. A. Julien, C. Mottillo and T. Friščić, *Green Chem.*, 2017, 2729–2747.
83 Q. Nawaz, M. A. U. Rehman, A. Burkovski, J. Schmidt, A. M. Beltrán, A. Shahid, N. K. Alber, W. Peukert and A. R. Boccaccini, *J. Mater. Sci. Mater. Med.*, 2018, **29**, 64.
84 C. Vichery and J. M. Nedelec, *Materials*, 2016, 288.
85 J. R. Jones, *Acta Biomater.*, 2015, S53–S82.
86 H. Tripathi, C. Rath, A. S. Kumar, P. P. Manna and S. P. Singh, *Mater. Sci. Eng. C*, 2019, **94**, 279–290.
87 K. Zheng and A. R. Boccaccini, *Adv. Colloid Interface Sci.*, 2017, **249**, 363–373.
88 M. Ojansivu, A. Rashad, A. Ahlinder, J. Massera, A. Mishra, K. Syverud, A. Finne-Wistrand, S. Miettinen and K. Mustafa, *Biofabrication*, 2019, **11**, 035010.
89 Á. J. Leite and J. F. Mano, *J. Mater. Chem. B*, 2017, **5**, 4555–4568.
90 Z. Neščáková, K. Zheng, L. Liverani, Q. Nawaz, D. Galusková, H. Kaňková, M. Michálek, D. Galusek and A. R. Boccaccini, *Bioact. Mater.*, 2019, **4**, 312–321.
91 C. Wen, Y. Hong, J. Wu, L. Luo, Y. Qiu and J. Ye, *RSC Adv.*, 2018, **8**, 14561–14569.
92 H. Luo, D. Ji, W. Li, J. Xiao, C. Li, G. Xiong, Y. Zhu and Y. Wan, *Mater. Chem. Phys.*, 2016, **176**, 1–5.

93 J. Bang, H. Lee, Y. Yang, J.-K. Oh and H. W. Kwak, *Polymers*, 2021, **13**, 636.
94 A. Anžlovar, A. Krajnc and E. Žagar, *Cellulose*, 2020, **27**, 5785–5800.
95 J. Lee and S. Y. Kwak, *ACS Omega*, 2018, **3**, 2634–2640.
96 X. Kesse, C. Vichery and J. M. Nedelec, *ACS Omega*, 2019, **4**, 5768–5775.
97 C. Y. Tsai, W. C. Chang, G. L. Chen, C. H. Chung, J. X. Liang, W. Y. Ma and T. N. Yang, *Nanoscale Res. Lett.*, 2015, **10**, 1–7.
98 A. Kushwaha, H. Tyagi and M. Aslam, *AIP Adv.*, 2013, **3**, 042110.
99 L. Valencia and H. N. Abdelhamid, *Carbohydr. Polym.*, 2019, **213**, 338–345.
100 Z. Fang, G. Hou, C. Chen and L. Hu, *Curr. Opin. Solid State Mater. Sci.*, 2019, **23**, 100764.
101 A. J. Benítez and A. Walther, *J. Mater. Chem. A*, 2017, 16003–16024.
102 X. Xu, J. Zhou, L. Jiang, G. Lubineau, T. Ng, B. S. Ooi, H.-Y. Liao, C. Shen, L. Chen and J. Y. Zhu, *Nanoscale*, 2016, **8**, 12294–12306.
103 R. Yin, S. Yang, Q. Li, S. Zhang, H. Liu, J. Han, C. Liu and C. Shen, *Sci. Bull.*, 2020, **65**, 899–908.
104 E. Morales-Narváez, H. Golmohammadi, T. Naghdi, H. Yousefi, U. Kostiv, D. Horák, N. Pourreza and A. Merkoçi, *ACS Nano*, 2015, **9**, 7296–7305.
105 N. Pourreza, H. Golmohammadi, T. Naghdi and H. Yousefi, *Biosens. Bioelectron.*, 2015, **74**, 353–359.
106 L. Lavoine and B. Nathalie, *J. Mater. Chem. A*, 2017, **5**, 16105–16117.
107 S. Gupta, F. Martoïa, L. Orgéas and P. Dumont, *Appl. Sci.*, 2018, **8**, 2463.
108 S. Deville, *Scr. Mater.*, 2018, **147**, 119–124.
109 P. Munier, V. Apostolopoulou-Kalkavoura, M. Persson and L. Bergström, *Cellulose*, 2020, **27**, 10825–10836.
110 S. Zhou, V. Apostolopoulou-Kalkavoura, M. V. Tavares da Costa, L. Bergström, M. Strømme and C. Xu, *Nano-Micro Lett.*, 2020, **12**, 1–13.
111 H. M. Yadav, J. D. Park, H. C. Kang, J. Kim and J. J. Lee, *Nanomater*, 2021, **11**, 395.
112 P. Wang, J. Zhao, R. Xuan, Y. Wang, C. Zou, Z. Zhang, Y. Wan and Y. Xu, *Dalt. Trans.*, 2014, **43**, 6762–6768.
113 L. Y. Ee and S. F. Yau Li, *Nanoscale Adv.*, 2021, **3**, 1167–1208.
114 X. Wang, Q. Wang and C. Xu, *Bioengineering*, 2020, 40.
115 P. Jiang, C. Yan, Y. Guo, X. Zhang, M. Cai, X. Jia, X. Wang and F. Zhou, *Biomater. Sci.*, 2019, **7**, 1805–1814.
116 G. Chinga-Carrasco, *Biomacromolecules*, 2018, 701–711.
117 M. W. Glasscott, A. D. Pendergast, M. H. Choudhury and J. E. Dick, *ACS Appl. Nano Mater.*, 2018, **2**, 819–830.
118 A. Balea, A. Blanco, M. D. Aguilar, M. C. Monte, Q. Tarrés, E. Fuente, P. Mutje and C. Negro, *BioResources*, 2021, **16**, 4382–4410.
119 T. Li, A. J. Senesi and B. Lee, *Chem. Rev.*, 2016, **116**, 11128–11180.
120 E. J. Foster, R. J. Moon, U. P. Agarwal, M. J. Bortner, J. Bras, S. Camarero-Espinosa, K. J. Chan, M. J. D. Clift, E. D. Cranston, S. J. Eichhorn, D. M. Fox, W. Y. Hamad, L. Heux, B. Jean, M. Korey, W. Nieh, K. J. Ong, M. S. Reid, S. Renneckar, R. Roberts, J. A. Shatkin, J. Simonsen, K. Stinson-Bagby, N. Wanasekara and J. Youngblood, *Chem. Soc. Rev.*, 2018, **47**, 2609–2679.
121 K. Ganguly, D. K. Patel, S. D. Dutta and K.-T. Lim, *ACS Omega*, 2021, **6**, 12424–12431.
122 F. Jiang, S. Hu and Y. Hsieh, *ACS Appl. Nano Mater.*, 2018, **1**, 6701–6710.
123 U. Goikuria, A. Larrañaga, E. Lizundia and J. L. Vilas, *J. Appl. Polym. Sci.*, 2021, **138**, 50639.
124 S. Yang, B. Xue, Y. Li, X. Li, L. Xie, S. Qin, K. Xu and Q. Zheng, *Chem. Eng. J.*, 2020, **383**, 123072.
125 T. Rosén, R. Wang, H. He, C. Zhan, S. Chodankar and B. S. Hsiao, *Nanoscale Adv.*, 2021, **3**, 4940–4951.
126 R. Kádár, S. Spirk and T. Nypelö, *ACS Nano*, 2021, **15**, 7931–7945.
127 Y. Mao, K. Liu, C. Zhan, L. Geng, B. Chu and B. S. Hsiao, *J. Phys. Chem. B*, 2017, **121**, 1340–1351.
128 V. Esquivel-Peña, V. Guccini, S. Kumar, G. Salazar-Alvarez, E. R. de S. Miguel and J. de Gyves, *RSC Adv.*, 2020, **10**, 12460–12468.
129 J. Van Rie, G. González-Rubio, S. Kumar, C. Schütz, J. Kohlbrecher, M. Vanroelen, T. Van Gerven, O. Deschaume, C. Bartic, L. M. Liz-Marzán, G. Salazar-Alvarez and W. Thielemans, *Chem. Commun.*, 2020, **56**, 13001–13004.
130 T. Nypelö, H. Pynnönen, M. Österberg, J. Paltakari and J. Laine, *Cellul*, 2012, **19**, 779–792.
131 A. P. Carapeto, A. M. Ferraria and A. M. B. do Rego, *Nanomater*, 2019, **9**, 780.
132 D. Kim, S. Park, I. Jo, S.-M. Kim, D. H. Kang, S.-P. Cho, J. B. Park, B. H. Hong and M.-H. Yoon, *Small*, 2017, **13**, 1700331.
133 M. Sedighi, M. N. Boone, J. L. Fife, S. Zhao, M. M. Koebel, T. Zimmermann and P. Tingaut, *Compos. Sci. Technol.*, 2016, **124**, 71–80.
134 A. B. Poma, M. Chwastyk and M. Cieplak, *Cellul*, 2016, **23**, 1573–1591.
135 J. Wohlert and L. A. Berglund, *J. Chem. Theory Comput.*, 2011, **7**, 753–760.
136 G. Srinivas, X. Cheng and J. C. Smith, *J. Phys. Chem. B*, 2014, **118**, 3026–3034.
137 C. A. López, G. Bellesia, A. Redondo, P. Langan, S. P. S. Chundawat, B. E. Dale, S. J. Marrink and S. Gnanakaran, *J. Phys. Chem. B*, 2015, **119**, 465–473.
138 S. Mani, D. J. Cosgrove and G. A. Voth, *J. Phys. Chem. B*, 2020, **124**, 3527–3539.
139 J. Tersoff, *Phys. Rev. Lett.*, 1988, **61**, 2879.
140 D. W. Brenner, *Phys. Rev. B*, 1990, **42**, 9458.
141 M. T. Knippenberg, P. T. Mikulski, K. E. Ryan, S. J. Stuart, G. Gao and J. A. Harrison, *J. Chem. Phys.*, 2012, **136**, 164701.
142 T. Liang, T. R. Shan, Y. T. Cheng, B. D. Devine, M. Noordhoek, Y. Li, Z. Lu, S. R. Phillpot and S. B. Sinnott, *Mater. Sci. Eng. R Reports*, 2013, **74**, 255–279.
143 S. J. Stuart, A. B. Tutein and J. A. Harrison, *J. Chem. Phys.*, 2000, **112**, 6472.
144 A. C. T. van Duin, S. Dasgupta, F. Lorant and W. A. Goddard III, *J. Phys. Chem. A*, 2001, **105**, 9396–9409.

145 T. P. Senftle, S. Hong, M. M. Islam, S. B. Kylasa, Y. Zheng, Y. K. Shin, C. Junkermeier, R. Engel-Herbert, M. J. Janik, H. M. Aktulga, T. Verstraelen, A. Grama and A. C. T. van Duin, *npj Comput. Mater.*, 2016, **2**, 1–14.
146 M. Zheng, Z. Wang, X. Li, X. Qiao, W. Song and L. Guo, *Fuel*, 2016, **177**, 130–141.
147 L. Atmani, P.-L. Valdenaire, R. J.-M. Pellenq, C. Bichara, H. van Damme, A. van Duin, F. Ulm and J.-M. Leyssale, *Energy Fuels*, 2020, **34AD**, 1537–1547.
148 L. Atmani, C. Bichara, R. J.-M. Pellenq, H. Van Damme, A. C. T. van Duin, Z. Raza, L. A. Truflandier, A. Obliger, P. G. Kralert, F. J. Ulm and J.-M. Leyssale, *Chem. Sci.*, 2017, **8**, 8325–8335.
149 P.-L. Valdenaire, R. J. M. Pellenq, F. J. Ulm, A. C. T. Van Duin, J.-M. Leyssale, R. J. M. Pellenq and F. J. Ulm, *J. Chem. Phys.*, 2020, **152**, 024123.
150 C. Zhu, S. Monti and A. P. Mathew, *ACS Nano*, 2018, **12**, 7028–7038.
151 E. Ahmed and A. Rothenberger, *Microporous Mesoporous Mater.*, 2016, **220**, 247–252.
152 J. Patricio, A. Angelis-Dimakis, A. Castillo-Castillo, Y. Kalmykova and L. Rosado, *J. CO2 Util.*, 2017, **17**, 50–59.
153 J. Hennessy, *Nat. Mater.*, 2015, **14**, 857.
154 T. L. Church, A. B. Jasso-Salcedo, F. Björnerbäck and N. Hedin, *Sci. China Chem.*, 2017, **60**, 1033–1055.
155 Y. Feng, H. Wang and J. Yao, *Coord. Chem. Rev.*, 2021, **431**, 213677.
156 C. Lei, J. Gao, W. Ren, Y. Xie, S. Y. H. Abdalkarim, S. Wang, Q. Ni and J. Yao, *Carbohydr. Polym.*, 2019, **205**, 35–41.
157 L. Valencia and H. N. Abdelhamid, *Carbohydr. Polym.*, 2019, **213**, 338–345.
158 Z. Bacsik, O. Cheung, P. Vasiliev and N. Hedin, *Appl. Energy*, 2016, **162**, 613–621.
159 D. O. Ojwang, J. Grins and G. Svensson, *Microporous Mesoporous Mater.*, 2018, **272**, 70–78.
160 L. Keshavarz, M. R. Ghaani, J. M. D. MacElroy and N. J. English, *Chem. Eng. J.*, 2021, **412**, 128604.
161 M. Anas, A. G. Gönel, S. E. Bozbag and C. Erkey, *J. CO2 Util.*, 2017, **21**, 82–88.
162 Y. Chen, L. Zhang, Y. Yang, B. Pang, W. Xu, G. Duan, S. Jiang and K. Zhang, *Adv. Mater.*, 2021, **33**, 2005569.
163 S. Zhou, M. Strømme and C. Xu, *Chem.–Eur. J.*, 2019, **25**, 3515–3520.
164 B. Abdulla, *Nanocellulose Surface Functionalization for In Situ Growth of Zeolitic Imidazolate Framework 67 and 8*, 2020.
165 X. F. Zhang, T. Hou, J. Chen, Y. Feng, B. Li, X. Gu, M. He and J. Yao, *ACS Appl. Mater. Interfaces*, 2018, **10**, 24930–24936.
166 M. Jia, X. F. Zhang, Y. Feng, Y. Zhou and J. Yao, *J. Memb. Sci.*, 2020, **595**, 117579.
167 X. F. Zhang, Y. Feng, Z. Wang, M. Jia and J. Yao, *J. Memb. Sci.*, 2018, **568**, 10–16.
168 S. Sinquefield, P. N. Ciesielski, K. Li, D. J. Gardner and S. Ozcan, *ACS Sustain. Chem. Eng.*, 2020, **8**, 9601–9615.
169 M. Mubashir, Y. F. Yeong, K. K. Lau, T. L. Chew and J. Norwahyu, *Sep. Purif. Technol.*, 2018, **199**, 140–151.
170 W. Guan, Y. Dai, C. Dong, X. Yang and Y. Xi, *J. Appl. Polym. Sci.*, 2020, **137**, 48968.
171 C. Moser, H. Backlund, L. Drenth, G. Henriksson and M. E. Lindström, *Nord. Pulp Pap. Res. J.*, 2018, **33**, 186–193.
172 G. W. Sears, *Anal. Chem.*, 1956, **28**, 1981–1983.
173 R. D. C. Soltani, M. Mashayekhi, M. Naderi, G. Boczkaj, S. Jorfi and M. Safari, *Ultrason. Sonochem.*, 2019, **55**, 117–124.
174 Y. Hosakun, K. Halász, M. Horváth, L. Csóka and V. Djoković, *Chem. Eng. J.*, 2017, **324**, 83–92.
175 C. Xin, M. Hu, K. Wang and X. Wang, *Langmuir*, 2017, **33**, 6667–6676.
176 L. Valencia, W. Rosas-Arbelaez, A. Aguilar-Sánchez, A. P. Mathew and A. E. C. Palmqvist, *ACS Appl. Mater. Interfaces*, 2019, **11**, 40424–40431.
177 S. Ma, M. Zhang, J. Nie, J. Tan, S. Song and Y. Luo, *Carbohydr. Polym.*, 2019, **208**, 328–335.
178 S. Ma, M. Zhang, J. Nie, B. Yang, S. Song and P. Lu, *Cellulose*, 2018, **25**, 5999–6010.
179 X. Ma, Y. Lou, X.-B. Chen, Z. Shi and Y. Xu, *Chem. Eng. J.*, 2019, **356**, 227–235.
180 L. Zhu, L. Zong, X. Wu, M. Li, H. Wang, J. You and C. Li, *ACS Nano*, 2018, **12**, 4462–4468.
181 Z. Su, M. Zhang, Z. Lu, S. Song, Y. Zhao and Y. Hao, *Cellulose*, 2018, **25**, 1997–2008.
182 Z. Wang, L. Song, Y. Wang, X. F. Zhang, D. Hao, Y. Feng and J. Yao, *Chem. Eng. J.*, 2019, **371**, 138–144.
183 J. Li, S. Tan and Z. Xu, *Nanomaterials*, 2020, **10**, 1–13.
184 G. Chen, W. J. Koros and C. W. Jones, *ACS Appl. Mater. Interfaces*, 2016, **8**, 9700–9709.
185 D. S. Malik, C. K. Jain and A. K. Yadav, *Appl. Water Sci.*, 2017, **7**, 2113–2136.
186 A. W. Carpenter, C. F. De Lannoy and M. R. Wiesner, *Environ. Sci. Technol.*, 2015, **49**, 5277–5287.
187 R. E. Abouzeid, R. Khiari, N. El-Wakil and A. Dufresne, *Biomacromolecules*, 2019, **20**, 573–597.
188 Z. Karim, S. Claudpierre, M. Grahn, K. Oksman and A. P. Mathew, *J. Memb. Sci.*, 2016, **514**, 418–428.
189 P. Liu, K. Oksman and A. P. Mathew, *J. Colloid Interface Sci.*, 2016, **464**, 175–182.
190 C. Santhosh, A. Malathi, E. Dhaneshvar, A. Bhatnagar, A. N. Grace and J. Madhavan, in *Nanoscale Materials in Water Purification*, Elsevier, 2018, pp. 431–446.
191 J. Lu, R. N. Jin, C. Liu, Y. F. Wang and X. kun Ouyang, *Int. J. Biol. Macromol.*, 2016, **93**, 547–556.
192 A. Alipour, S. Zarinabadi, A. Azimi and M. Mirzaei, *Int. J. Biol. Macromol.*, 2020, **151**, 124–135.
193 N. Amiralian, M. Mustapic, M. S. A. Hossain, C. Wang, M. Konarova, J. Tang, J. Na, A. Khan and A. Rowan, *J. Hazard. Mater.*, 2020, **394**, 122571.
194 P. Cruz-Tato, E. O. Ortiz-Quiles, K. Vega-Figueroa, L. Santiago-Martoral, M. Flynn, L. M. Díaz-Vázquez and E. Nicolau, *Environ. Sci. Technol.*, 2017, **51**, 4585–4595.
195 T. Hashem, A. H. Ibrahim, C. Wöll and M. H. Alkordi, *ACS Appl. Nano Mater.*, 2019, **2**, 5804–5808.
196 L. Mo, Y. Shen, Y. Tan and S. Zhang, *Int. J. Biol. Macromol.*, 2021, **193**, 1488–1498.

197 H. Gu, X. Zhou, S. Lyu, D. Pan, M. Dong, S. Wu, T. Ding, X. Wei, I. Seok, S. Wei and Z. Guo, *J. Colloid Interface Sci.*, 2020, **560**, 849–856.
198 C. Tang, P. Brodie, Y. Li, N. J. Grishkewich, M. Brunsting and K. C. Tam, *Chem. Eng. J.*, 2020, **392**, 124821.
199 C. Tang, P. Brodie, M. Brunsting and K. C. Tam, *Carbohydr. Polym.*, 2020, **242**, 116397.
200 M. KarzarJeddi, O. Laitinen, M. Mahkam and H. Liimatainen, *Mater. Des.*, 2020, **196**, 109106.
201 N. Mohammed, N. Grishkewich, R. M. Berry and K. C. Tam, *Cellulose*, 2015, **22**, 3725–3738.
202 W. Zhang, X. Wang, Y. Zhang, B. van Bochove, E. Mäkilä, J. Seppälä, W. Xu, S. Willför and C. Xu, *Sep. Purif. Technol.*, 2020, **242**, 116523.
203 S. Chatterjee, W. T. Ke and Y. C. Liao, *J. Taiwan Inst. Chem. Eng.*, 2020, **111**, 261–269.
204 M. Karzar Jeddi, O. Laitinen and H. Liimatainen, *Mater. Des.*, 2019, **183**, 108115.
205 N. Halib, F. Perrone, M. Cemazar, B. Dapas, R. Farra, M. Abrami, G. Chiarappa, G. Forte, F. Zanconati, G. Pozzato, L. Murena, N. Fiotti, R. Lapasin, L. Cansolino, G. Grassi and M. Grassi, *Materials*, 2017, DOI: 10.3390/ma10080977.
206 G. F. Picheth, C. L. Pirich, M. R. Sierakowski, M. A. Woehl, C. N. Sakakibara, C. F. de Souza, A. A. Martin, R. da Silva and R. A. de Freitas, *Int. J. Biol. Macromol.*, 2017, **104**, 97–106.
207 M. Jorfi and E. J. Foster, *J. Appl. Polym. Sci.*, 2015, **132**, 41719.
208 H. Seddiqi, E. Oliaei, H. Honarkar, J. Jin, L. C. Geonzon, R. G. Bacabac and J. Klein-Nulend, *Cellulose*, 2021, **28**, 1893–1931.
209 H. Du, W. Liu, M. Zhang, C. Si, X. Zhang and B. Li, *Carbohydr. Polym.*, 2019, **209**, 130–144.
210 M. Oprea and S. I. Voicu, *Carbohydr. Polym.*, 2020, **247**, 116683.
211 T. S. Anirudhan, S. S. Nair and C. Sekhar, *J. Memb. Sci.*, 2017, **539**, 344–357.
212 A. Fakhri, S. Tahami and P. A. Nejad, *J. Photochem. Photobiol. B Biol.*, 2017, **175**, 83–88.
213 M. Lu, Y. Cui, S. Zhao and A. Fakhri, *J. Photochem. Photobiol. B Biol.*, 2020, **205**, 111842.
214 A. Manafi Khajeh Pasha, M. Hosseini, A. Fakhri, V. K. Gupta and S. Agarwal, *J. Mol. Liq.*, 2019, **289**, 110950.
215 D. Pathania, M. Kumari and V. K. Gupta, *Mater. Des.*, 2015, **87**, 1056–1064.
216 S. A. Noorian, N. Hemmatinejad and J. A. R. Navarro, *J. Inorg. Biochem.*, 2019, **201**, 110818.
217 M. Alavi and A. Nokhodchi, *Macromol. Biosci.*, 2020, **20**, 1900362.
218 V. Kanikireddy, K. Varaprasad, T. Jayaramudu, C. Karthikeyan and R. Sadiku, *Int. J. Biol. Macromol.*, 2020, **164**, 963–975.
219 W. He, J. Wu, J. Xu, D. A. Mosselhy, Y. Zheng and S. Yang, *Adv. Wound Care*, 2020, **10**, 623–640.
220 A. A. Aly and M. K. Ahmed, *Int. J. Pharm.*, 2021, **598**, 120325.
221 E. Pinho and G. Soares, *J. Mater. Chem. B*, 2018, **6**, 1887–1898.
222 C. Duan, J. Meng, X. Wang, X. Meng, X. Sun, Y. Xu, W. Zhao and Y. Ni, *Carbohydr. Polym.*, 2018, **193**, 82–88.
223 J. Wu, Y. Zheng, W. Song, J. Luan, X. Wen, Z. Wu, X. Chen, Q. Wang and S. Guo, *Carbohydr. Polym.*, 2014, **102**, 762–771.
224 X. Bie, M. Q. Khan, A. Ullah, S. Ullah, D. Kharaghani, D.-N. Phan, Y. Tamada and I. S. Kim, *Mater. Res. Express*, 2020, **7**, 45004.
225 C. S. Ong, L. Nam, K. Ong, A. Krishnan, C. Y. Huang, T. Fukunishi and N. Hibino, *Biomed Res. Int.*, 2018, **2018**, 6497242.
226 F. Wahid, Y.-X. Duan, X.-H. Hu, L.-Q. Chu, S.-R. Jia, J.-D. Cui and C. Zhong, *Int. J. Biol. Macromol.*, 2019, **132**, 692–700.
227 X. Wang, F. Cheng, J. Liu, J.-H. Smått, D. Gepperth, M. Lastusaari, C. Xu and L. Hupa, *Acta Biomater.*, 2016, **46**, 286–298.
228 A. S. Elfeky, S. S. Salem, A. S. Elzaref, M. E. Owda, H. A. Eladawy, A. M. Saeed, M. A. Awad, R. E. Abou-Zeid and A. Fouda, *Carbohydr. Polym.*, 2020, **230**, 115711.
229 X. Nie, S. Wu, A. Mensah, Q. Wang, F. Huang, D. Li and Q. Wei, *J. Colloid Interface Sci.*, 2020, **579**, 233–242.
230 C. Duan, X. Meng, C. Liu, W. Lu, J. Liu, L. Dai, W. Wang, W. Zhao, C. Xiong and Y. Ni, *Carbohydr. Polym.*, 2019, **222**, 115042.
231 H. Jafari, M. Shahrousvand and B. Kaffashi, *ACS Biomater. Sci. Eng.*, 2018, **4**, 2484–2493.
232 A. Cañas-Gutiérrez, E. Martinez-Correa, D. Suárez-Avendaño, D. Arboleda-Toro and C. Castro-Herazo, *Cellulose*, 2020, **27**, 10747–10763.
233 Y. Hu, Y. Zhu, X. Zhou, C. Ruan, H. Pan and J. M. Catchmark, *J. Mater. Chem. B*, 2016, **4**, 1235–1246.
234 S. Y. H. Abdalkarim, H.-Y. Yu, C. Wang, L. Yang, Y. Guan, L. Huang and J. Yao, *ACS Appl. Bio Mater.*, 2018, **1**, 714–727.
235 J. Yang, M. Du, L. Wang, S. Li, G. Wang, X. Yang, L. Zhang, Y. Fang, W. Zheng, G. Yang and X. Jiang, *ACS Appl. Mater. Interfaces*, 2018, **10**, 33049–33059.
236 S. Kamel and T. A. Khattab, *Biosens*, 2020, **10**, 67.
237 N. P. Shetti, S. D. Bukkitgar, K. R. Reddy, C. V. Reddy and T. M. Aminabhavi, *Colloids Surfaces B Biointerfaces*, 2019, **178**, 385–394.
238 K. B. R. Teodoro, F. L. Migliorini, W. A. Christinelli and D. S. Correa, *Carbohydr. Polym.*, 2019, **212**, 235–241.
239 C. L. Pirich, R. A. de Freitas, R. M. Torresi, G. F. Picheth and M. R. Sierakowski, *Biosens. Bioelectron.*, 2017, **92**, 47–53.
240 D. Li, K. Ao, Q. Wang, P. Lv and Q. Wei, *Mol*, 2016, **21**, 618.
241 M. Vasudevan, M. J. Y. Tai, V. Perumal, S. C. B. Gopinath, S. S. Murthe, M. Ovinis, N. M. Mohamed and N. Joshi, *J. Taiwan Inst. Chem. Eng.*, 2021, **118**, 245–253.
242 K. Ratajczak and M. Stobiecka, *Carbohydr. Polym.*, 2020, **229**, 115463.
243 R. Tian, Y. Li and J. Bai, *Anal. Chim. Acta*, 2019, **1058**, 89–96.
244 N. Colozza, V. Caratelli, D. Moscone and F. Arduini, *Biosens*, 2021, **11**, 328.
245 T. Pinheiro, J. Ferrão, A. C. Marques, M. J. Oliveira, N. M. Batra, P. M. F. J. Costa, M. P. Macedo, H. Águas, R. Martins and E. Fortunato, *Nanomater*, 2020, **10**, 2027.

246 J. H. Kim, S. Mun, H.-U. Ko, G.-Y. Yun and J. Kim, *Nanotechnology*, 2014, **25**, 92001.
247 D. Hu and W. Ma, *Ind. Eng. Chem. Res.*, 2020, **59**, 19465–19484.
248 B. Pang, G. Jiang, J. Zhou, Y. Zhu, W. Cheng, D. Zhao, K. Wang, G. Xu and H. Yu, *Adv. Electron. Mater.*, 2021, **7**, 2000944.
249 S. Nie, N. Hao, K. Zhang, C. Xing and S. Wang, *Cellul*, 2020, **278**(27), 4173–4187.
250 P. Tayeb and A. H. Tayeb, *Carbohydr. Polym.*, 2019, **244**, 115149.
251 R. Sabo, A. Yermakov, C. T. Law and R. Elhajjar, *J. Renew. Mater.*, 2016, **4**, 297–312.
252 F. Hoeng, A. Denneulin and J. Bras, *Nanoscale*, 2016, **8**, 13131–13154.
253 Z. Chen, T. Yan and Z. Pan, *Cellul*, 2020, (28), 615–645.
254 Y. Xie, Y. Zheng, J. Fan, Y. Wang, L. Yue and N. Zhang, *ACS Appl. Mater. Interfaces*, 2018, **10**, 22692–22702.
255 N. Song, H. Pan, X. Liang, D. Cao, L. Shi and P. Ding, *J. Mater. Chem. C*, 2018, **6**, 7085–7091.
256 C. Gao, S. Yuan, K. Cui, Z. Qiu, S. Ge, B. Cao and J. Yu, *Sol. RRL*, 2018, **2**, 1800175.
257 F. B. Kadumudi, J. Trifol, M. Jahanshahi, T.-G. Zsurzsan, M. Mehrali, E. Zeqiraj, H. Shaki, M. Alehosseini, C. Gundlach, Q. Li, M. Dong, M. Akbari, A. Knott, K. Almdal and A. Dolatshahi-Pirouz, *ACS Appl. Mater. Interfaces*, 2020, **12**, 48027–48039.
258 R. Barras, I. Cunha, D. Gaspar, E. Fortunato, R. Martins and L. Pereira, *Flex. Print. Electron.*, 2017, **2**, 014006.
259 Y. H. Jung, T.-H. Chang, H. Zhang, C. Yao, Q. Zheng, V. W. Yang, H. Mi, M. Kim, S. J. Cho, D.-W. Park, H. Jiang, J. Lee, Y. Qiu, W. Zhou, Z. Cai, S. Gong and Z. Ma, *Nat. Commun.*, 2015, **6**, 7170.
260 E. Lizundia, M. Delgado-Aguilar, P. Mutjé, E. Fernández, B. Robles-Hernandez, M. R. de la Fuente, J. L. Vilas and L. M. León, *Cellul*, 2016, **233**, 1997–2010.
261 S. Ji, J. Jang, E. Cho, S.-H. Kim, E.-S. Kang, J. Kim, H.-K. Kim, H. Kong, S.-K. Kim, J.-Y. Kim and J.-U. Park, *Adv. Mater.*, 2017, **29**, 1700538.
262 S. Zhang, H. Liu, S. Yang, X. Shi, D. Zhang, C. Shan, L. Mi, C. Liu, C. Shen and Z. Guo, *ACS Appl. Mater. Interfaces*, 2019, **11**, 10922–10932.
263 H. Y. Choi, T. W. Lee, S. E. Lee, J. D. Lim and Y. G. Jeong, *Compos. Sci. Technol.*, 2017, **150**, 45–53.
264 Y. Chen, L. Pang, Y. Li, H. Luo, G. Duan, C. Mei, W. Xu, W. Zhou, K. Liu and S. Jiang, *Compos. Part A Appl. Sci. Manuf.*, 2020, **135**, 105960.
265 P. Sahatiya, A. Kadu, H. Gupta, P. T. Gomathi and S. Badhulika, *ACS Appl. Mater. Interfaces*, 2018, **10**, 9048–9059.
266 P. T. Gomathi, P. Sahatiya and S. Badhulika, *Adv. Funct. Mater.*, 2017, **27**, 1701611.
267 D. Zhao, Y. Zhu, W. Cheng, W. Chen, Y. Wu and H. Yu, *Adv. Mater.*, 2021, **33**, 2000619.
268 A. Malti, R. Brooke, X. Liu, D. Zhao, P. A. Ersman, M. Fahlman, M. P. Jonsson, M. Berggren and X. Crispin, *J. Mater. Chem. C*, 2016, **4**, 9680–9686.
269 S. Thiemann, S. J. Sachnov, F. Pettersson, R. Bollström, R. Österbacka, P. Wasserscheid and J. Zaumseil, *Adv. Funct. Mater.*, 2014, **24**, 625–634.
270 H. Oh, S. S. Kwak, B. Kim, E. Han, G.-H. Lim, S.-W. Kim and B. Lim, *Adv. Funct. Mater.*, 2019, **29**, 1904066.
271 B. W. An, S. Heo, S. Ji, F. Bien and J.-U. Park, *Nat. Commun.*, 2018, **91**(9), 1–10.
272 H. Wang, Y. Pei, X. Qian and X. An, *Carbohydr. Polym.*, 2020, **236**, 116030.
273 Q. Fu, Y. Chen and M. Sorieul, *ACS Nano*, 2020, **14**, 3528–3538.
274 Z. Fang, H. Zhu, C. Preston, X. Han, Y. Li, S. Lee, X. Chai, G. Chen and L. Hu, *J. Mater. Chem. C*, 2013, **1**, 6191–6197.
275 S. Darabi, M. Hummel, S. Rantasalo, M. Rissanen, I. Ö. Månsson, H. Hilke, B. Hwang, M. Skrifvars, M. M. Hamedi, H. Sixta, A. Lund and C. Müller, *ACS Appl. Mater. Interfaces*, 2020, **12**, 56403–56412.
276 M. B. Majewski, A. W. Peters, M. R. Wasielewski, J. T. Hupp and O. K. Farha, *ACS Energy Lett*, 2018, **3**, 598–611.
277 T. Qiu, Z. Liang, W. Guo, H. Tabassum, S. Gao and R. Zou, *ACS Energy Lett*, 2020, **5**, 520–532.
278 D. Sheberla, L. Sun, M. A. Blood-Forsythe, S. Er, C. R. Wade, C. K. Brozek, A. Aspuru-Guzik and M. Dinca, *J. Am. Chem. Soc.*, 2014, **136**, 8859–8862.
279 W. Zhang, B. Zheng, W. Shi, X. Chen, Z. Xu, S. Li, Y. R. Chi, Y. Yang, J. Lu, W. Huang and F. Huo, *Adv. Mater.*, 2018, **30**, 1800643.
280 W. Xia, A. Mahmood, R. Zou and Q. Xu, *Energy Environ. Sci.*, 2015, **8**, 1837–1866.
281 H. Furukawa, K. E. Cordova, M. O'Keeffe and O. M. Yaghi, *Science*, 2013, **341**, 1230444.
282 K. J. Lee, J. H. Lee, S. Jeoung and H. R. Moon, *Acc. Chem. Res.*, 2017, **50**, 2684–2692.
283 Z. Liang, C. Qu, W. Guo, R. Zou and Q. Xu, *Adv. Mater.*, 2018, **30**, 1702891.
284 S. Zhou, X. Kong, B. Zheng, F. Huo, M. Strømme and C. Xu, *ACS Nano*, 2019, **13**, 9578–9586.
285 L. Wang, X. Feng, L. Ren, Q. Piao, J. Zhong, Y. Wang, H. Li, Y. Chen and B. Wang, *J. Am. Chem. Soc.*, 2015, **137**, 4920–4923.
286 J. L. Zhuang, D. Ar, X. J. Yu, J. X. Liu and A. Terfort, *Adv. Mater.*, 2013, **25**, 4631–4635.
287 L. Sun, M. G. Campbell and M. Dince, *Angew. Chem., Int. Ed.*, 2016, **55**, 3566–3579.
288 J. Park, A. C. Hinckley, Z. Huang, D. Feng, A. A. Yakovenko, M. Lee, S. Chen, X. Zou and Z. Bao, *J. Am. Chem. Soc.*, 2018, **140**, 14533–14537.
289 G. Wu, J. Huang, Y. Zang, J. He and G. Xu, *J. Am. Chem. Soc.*, 2017, **139**, 1360–1363.
290 S. Zhou, Z. Qiu, M. Strømme and C. Xu, *Energy Environ. Sci.*, 2021, **14**, 900–905.
291 C. Xu, X. Kong, S. Zhou, B. Zheng, F. Huo and M. Strømme, *J. Mater. Chem. A*, 2018, **6**, 24050–24057.
292 D. Lin, Y. Liu and Y. Cui, *Nat. Nanotechnol.*, 2017, **12**, 194–206.
293 C. P. Grey and J. M. Tarascon, *Nat. Mater.*, 2016, **16**, 45–56.

294 N. Ojha, N. Pradhan, S. Singh, A. Barla, A. Shrivastava, P. Khatua, V. Rai and S. Bose, *Sci. Rep.*, 2017, **7**, 39515.
295 G. Harper, R. Sommerville, E. Kendrick, L. Driscoll, P. Slater, R. Stolkin, A. Walton, P. Christensen, O. Heidrich, S. Lambert, A. Abbott, K. Ryder, L. Gaines and P. Anderson, *Nature*, 2019, **575**, 75–86.
296 S. K. Kang, R. K. J. Murphy, S. W. Hwang, S. M. Lee, D. V. Harburg, N. A. Krueger, J. Shin, P. Gamble, H. Cheng, S. Yu, Z. Liu, J. G. McCall, M. Stephen, H. Ying, J. Kim, G. Park, R. C. Webb, C. H. Lee, S. Chung, D. S. Wie, A. D. Gujar, B. Vemulapalli, A. H. Kim, K. M. Lee, J. Cheng, Y. Huang, S. H. Lee, P. V. Braun, W. Z. Ray and J. A. Rogers, *Nature*, 2016, **530**, 71–76.
297 A. H. Havelaar, M. D. Kirk, P. R. Torgerson, H. J. Gibb, T. Hald, R. J. Lake, N. Praet, D. C. Bellinger, N. R. de Silva, N. Gargouri, N. Speybroeck, A. Cawthorne, C. Mathers, C. Stein, F. J. Angulo, B. Devleesschauwer, G. O. Adegoke, R. Afshari, D. Alasfoor, J. Baines, K. Balakrishnan, W. M. Bin Hamza, R. E. Black, P. M. Bolger, W. Chaicumpa, A. Cravioto, D. Döpfer, J. E. Ehiri, A. Fazil, C. Ferreccio, E. M. Fèvre, G. Hall, F. Kasuga, K. H. Keddy, C. F. Lanata, H. Lei, X. Liu, B. Manyindo, G. Nasinyama, P. Ongolo-Zogo, J. I. Pitt, M. B. Rokni, B. Sripa, R. van Leeuwen, P. Verger, A. L. Willingham, X. N. Zhou, W. Aspinall, R. Buchanan, C. Budke, M. L. Caipo, H. Carabin, D. Cole, R. M. Cooke, J. A. Crump, F. El-Jardali, C. Fischer-Walker, T. Fürst, J. A. Haagsma, A. J. Hall, O. Henao, S. Hoffmann, H. Jensen, N. Jessani, M. P. G. Koopmans, M. M. Levine, C. M. de Noordhout, S. Majowicz, S. A. McDonald, S. Pires, E. Scallan, B. Sripa, M. K. Thomas, L. Verhoef, F. Wu and M. Zeilmaker, *PLoS Med*, 2015, **12**, e1001923.
298 S. L. Brennan-Olsen, S. Cook, M. T. Leech, S. J. Bowe, P. Kowal, N. Naidoo, I. N. Ackerman, R. S. Page, S. M. Hosking, J. A. Pasco and M. Mohebbi, *BMC Musculoskelet. Disord.*, 2017, **18**, 271.
299 M. Tsang, A. Armutlulu, A. W. Martinez, S. A. B. Allen and M. G. Allen, *Microsyst. Nanoeng.*, 2015, **1**, 1.
300 T. Sun, Z. J. Li, H. G. Wang, D. Bao, F. L. Meng and X. B. Zhang, *Angew. Chem., Int. Ed.*, 2016, **55**, 10662–10666.
301 Y. J. Kim, W. Wu, S. E. Chun, J. F. Whitacre and C. J. Bettinger, *Proc. Natl. Acad. Sci. U. S. A.*, 2013, **110**, 20912–20917.
302 K. Fu, Z. Wang, C. Yan, Z. Liu, Y. Yao, J. Dai, E. Hitz, Y. Wang, W. Luo, Y. Chen, M. Kim and L. Hu, *Adv. Energy Mater.*, 2016, **6**, 1502496.
303 N. Li, L. Qiao, J. He, S. Wang, L. Yu, P. Murto, X. Li and X. Xu, *Adv. Funct. Mater.*, 2021, **31**, 2008681.
304 W. Wei, Q. Guan, C. You, J. Yu, Z. Yuan, P. Qiang, C. Zhou, Y. Ren, Z. You and F. Zhang, *J. Mater. Chem. A*, 2020, **8**, 13927–13934.
305 S. Han, T.-P. Ruoko, J. Gladisch, J. Erlandsson, L. Wågberg, X. Crispin and S. Fabiano, *Adv. Sustain. Syst.*, 2020, **4**, 2000004.
306 N. Hu, Y. Xu, Z. Liu, M. Liu, X. Shao and J. Wang, *Carbohydr. Polym.*, 2020, **243**, 116480.
307 C. Zhang, L. Liu, L. Zhou, X. Yin, X. Wei, Y. Hu, Y. Liu, S. Chen, J. Wang and Z. L. Wang, *ACS Nano*, 2020, **14**, 7092–7100.
308 Y. Zi and Z. L. Wang, *APL Mater.*, 2017, **5**, 74103.
309 Z. Lin, J. Yan, Q. Cai, X. Wen, H. Dong and C. Mu, *Nanoscale*, 2019, **11**, 21917–21926.
310 C. Zhu, S. Monti and A. P. Mathew, *ACS Nano*, 2018, **12**, 7028–7038.
311 R. Zhang, C. Dahlström, H. Zou, J. Jonzon, M. Hummelgård, J. Örtegren, N. Blomquist, Y. Yang, H. Andersson, M. Olsen, M. Norgren, H. Olin and Z. L. Wang, *Adv. Mater.*, 2020, **32**, 2002824.

